Politecnico di Torino

Politecnico di Torino

Master's Thesis in Automotive Engineering

A.a. 2024/2025

Graduation Session October 2025

Supports distribution optimization for Printed Circuit Boards subject to vibration in motorsport applications

Supervisor:
Prof. Luigi Garibaldi

Candidate:
Laura Pellegrino

Abstract

This thesis, developed in collaboration with Marelli Europe S.p.A., addresses the optimization of the number and placement of supports for printed circuit boards subjected to vibration loads. In motorsport applications, the current practice relies heavily on the experience of designers to select the support layout, which may result in conservative designs with unnecessary supports. Establishing objective guidelines reduces the subjectivity of this choice, may lower weight and cost, and accelerates the design phase.

The study focuses on two of Marelli's data acquisition electronic control units, each consisting of two printed circuit boards. Finite element modeling is performed at multiple levels of detail, ranging from simplified models that do not require precise component positioning to detailed representations that consider the local distribution of mass and stiffness.

Then the simplified models are used in an optimization study to determine the most effective support layouts for rectangular boards. The outcome is a set of design guidelines that link the first natural frequency to the geometry, mass, and stiffness of the board and provide practical recommendations for the choice of the number and position of supports.

Table of Contents

List of Tables

List of Figures

List of Acronyms and Symbols

BU	Business Unit
CV	Coefficient of Variation
DUT	Device Under Test
ECAD	Electronic Computer Aided Design
ECU	Electronic Control Unit
FE	Finite Element
FR	Fire-Retardant
FRF	Frequency Response Function
FEM	Finite Element Mehod
IMS	Insulated Metal Substrate
PCB	Printed Circuit Board
PCA	Printed Circuit Assembly
PSD	Power Spectral Density
PTH	Plated Through-Hole
PWB	Printed Wiring Board
SD	Standard Deviation
SMT	Surface Mounted Technology
E	Young's modulus
ρ	density
ν	Poisson's ratio

ω	natural frequency [rad/s]
f	natural frequency [Hz]
V	volume
t	thickness
a	long side
b	short side
x_{Cu}	copper fraction
m	mass
λ	dimensionless natural frequency parameter
γ	mass per unit area

Chapter 1

Introduction

Electronic assemblies are fundamental in modern automotive and motorsport applications, where they must operate reliably under highly demanding environmental conditions. In motorsport, in particular, these devices are exposed to harsh environments characterized by elevated temperatures, intense vibration levels, and potential dust or water intrusion, which go beyond the requirements of standard automotive applications.

This thesis focuses on the vibration behavior of PCAs (Printed Circuit Assemblies) in motorsport applications, aiming to develop optimized mechanical support strategies that improve reliability while minimizing weight and cost. An understanding of PCAs is essential and is discussed in the following section.

1.1 Printed Circuit Assembly

PCAs (Printed Circuit Assemblies) are key building blocks in virtually all modern electronic products. A typical PCA is composed of a set of fundamental elements [1]:

- **Printed Circuit Board:** the board that mechanically supports the components and provides the necessary electrical interconnections;
- **Electronic components:** devices that handle electricity performing the required function;
- **Connectors:** one or more interfaces that electrically connect the assembly to the rest of the system;
- **Mechanical parts:** mounting hardware that attaches the assembly to the system, provides thermal paths, and stiffens the structure.

1.1.1 Printed Circuit Board

A Printed Circuit Board (PCB) is a plate used to place the elements of an electronic circuit and the interconnections between them (Figure 1.1).

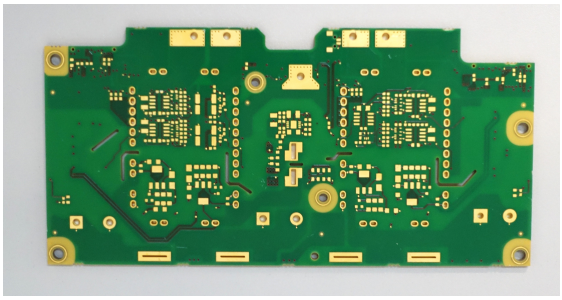

Figure 1.1: Printed Circuit Board example

The essential components of a printed circuit board are the substrate, a thin insulating board, either rigid or flexible, that provides mechanical support for conductors and components, and the wiring, generally high-purity copper traces attached to the substrate that form the electrical interconnections of the circuit.

A board that mechanically supports and electrically connects electronic components is also historically referred to as Printed Wiring Board (PWB). The term "printed" originates from the manufacturing process, where the conductive patterns are applied to the surface of the board using methods such as screen printing or photoengraving. These techniques are similar to those used to print graphics or text and are used to create circuit paths.

Classification by Number of Layers

Single-sided Printed Circuit Boards The wiring is available only on one side of the insulating substrate (Figure 1.2), the solder side, while the other side is called the component side. These types of board are inexpensive and easy to manufacture.

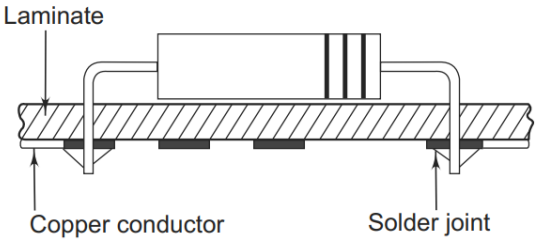

Figure 1.2: Single-sided PCB [2]

Double-sided Printed Circuit Boards Wiring patterns are present on both sides of the board. These types of PCB are used when component density and routing complexity exceed the capabilities of single-sided boards. Electrical connec-

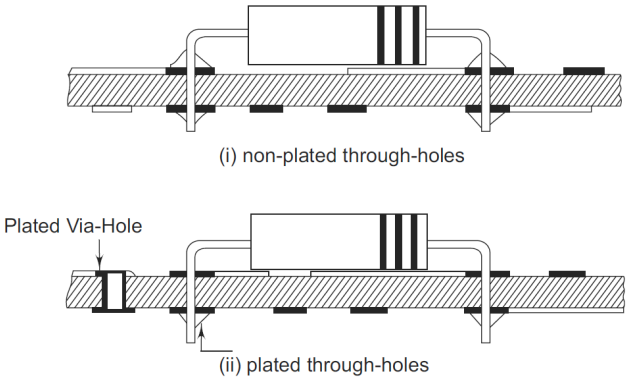

Figure 1.3: Double-sided PCB [2]

tion between the two sides of the insulating substrate can be achieved in two ways. In non-PTH (Plated Through-Hole) boards (Figure 1.3 (i)), the component leads are soldered on both sides of the board. In contrast, PTH boards (Figure 1.3 (ii)) use metallized holes that connect the circuitry on both sides by coating the inner walls of the drilled holes with a conductive material. The PTH approach is more complex and commonly used in high-density or multilayer PCB designs.

Multi-layer Boards They are used when the density of interconnections is too high to be managed with only two layers, or when specific electrical performance requirements exist, such as controlled impedance or improved electromagnetic shielding. In these cases, a simple two-sided layout is extended into a multi-layer configuration. A multi-layer board consists of multiple layers of conductive circuitry, typically in pairs, separated by insulating layers of so-called p̈repreg" material. These layers are stacked and laminated together forming sandwich-like structure, as illustrated in Figure 1.4.

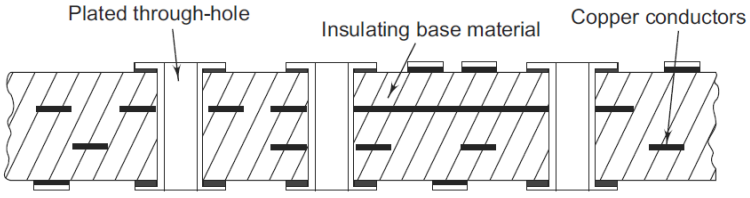

Figure 1.4: Cross-section of a multi-layer board with four layers [2]

Insulated Metal Substrate The IMS (Figure 1.5) is a PCB built on a metal plate, typically Aluminum, which is thermally conductive but electrically insulating. The metal plate serves both for thermal dissipation and for stiffening the board, making it more resistant to vibrations.

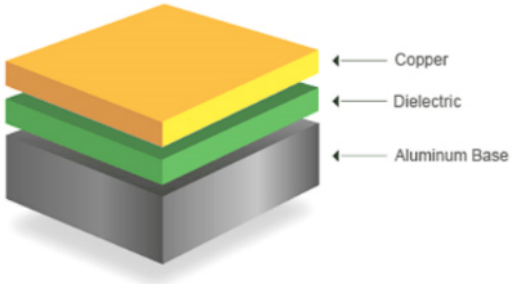

Figure 1.5: Insulated Metal Substrate PCB

Material-Based PCB Classification

The mechanical and electrical properties of a PCB are largely determined by the choice of substrate material. The substrate provides the structural support for copper traces and components, while its dielectric properties influence the electrical behavior of the circuit.

Glass-reinforced Epoxy Laminates. Rigid printed circuit boards are most commonly fabricated using glass-reinforced epoxy laminates, the standard example being FR4. This material is composed of woven glass fibers impregnated with epoxy resin, providing good mechanical strength, dimensional stability, and reliable electrical insulation over a wide temperature range.

Polyimide. Flexible PCBs are typically fabricated on polyimide-based films, such as Kapton®, which offer high thermal stability, chemical resistance, and the ability to withstand repeated bending without damaging the copper traces. These materials enable designs where the board can conform to three dimensional assemblies or accommodate dynamic motion.

Rigid, Flexible, and Rigid-Flex PCBs. Based on the substrate, PCBs are classified as rigid or flexible. Rigid boards are built with stiff laminates such as FR4, while flexible boards employ polyimide films that allow bending and folding. A hybrid category, rigid-flex boards, integrates rigid and flexible sections bonded together as shown in Figure 1.6. In these designs, components are typically mounted

on the rigid sections, while the flexible segments provide interconnection, enabling compact and mechanically robust assemblies.

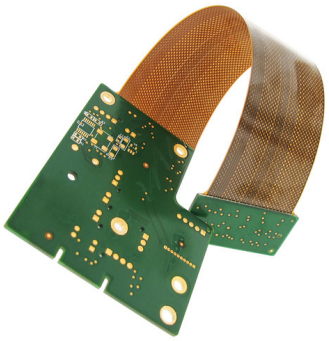

Figure 1.6: Rigid-Flex PCB example

1.1.2 Electronic Components

Electronic components vary widely in shape, size, and function. However, for the scope of this thesis, their electrical roles are not discussed in detail.

From a mechanical mounting perspective, components can be classified into two categories:

- **Through-hole components:** These have wire leads that are inserted into drilled holes in the board and soldered on the opposite side (Figure 1.7a).
- **Surface-mount components:** These are designed to be soldered directly onto the surface of the board without requiring drilled holes (Figure 1.7b).

Figure 1.7: Classification of components based on attachment method: (a) through-hole component; (b) surface-mount component [2].

1.1.3 Connectors

Connectors provide the electrical interface between a PCA and the rest of the system. Three main types of connectors can be individuated.

Board-to-board connectors

Board-to-board connectors can be classified according to the relative orientation of the connected PCBs (Figure 1.8) [3]:

Figure 1.8: Common board-to-board connector configurations: parallel (left), perpendicular (center), and horizontal (right) [3].

- **Parallel (Vertical or Mezzanine):** Both connectors are oriented vertically, allowing one board to be stacked directly on top of another. This configuration minimizes the footprint of the assembly.
- **Perpendicular (Motherboard-to-Daughterboard):** The connectors are mounted at 90° to each other. This arrangement is widely used in applications like storage devices, where several daughterboards are attached to a single motherboard to expand functionality in a compact volume.
- **Horizontal (Coplanar or Edge-to-Edge):** The connectors are oriented horizontally, keeping the mating plane low-profile with respect to the board surface. This is useful when height must be minimized.

External connectors

External connectors (Figure 1.9) provide the interface between the Electronic Control Unit (ECU) and external devices. They are used for signal transmission, enabling data exchange with sensors, actuators, and other subsystems.

Power connectors

When the electronic control unit also distributes electrical power, dedicated power connectors are employed, example in Figure 1.10. These connectors are specifically designed to handle higher currents.

Figure 1.9: External connectors

Figure 1.10: Power connector

1.1.4 Mechanical parts

Mountings

A further distinction concerns how the PCB is supported inside the electronic case. In Figure 1.11, two typical support methods are shown: on the right, the PCB is held by a rigid structure using clamps; on the left, it is supported by standoffs.

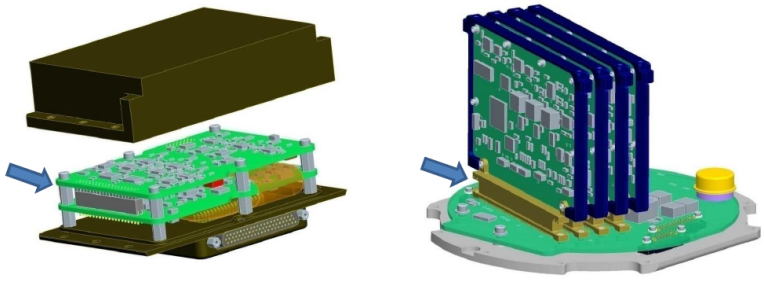

Figure 1.11: Typical PCB support methods: standoffs (left) and clamps (right) [4].

Thermal Pads

Thermal pads, also referred to as thermally conductive or interface pads, are solid materials designed to improve heat transfer from electronic components to a cooling element such as a heatsink or the case of the assembly [5]. By physically connecting the components to the ECU through materials characterized by higher thermal conductivity then air, they improve the thermal conduction (Figure 1.12).

Figure 1.12: Example of a thermal pad.

Most thermal pads are silicone-based, which provides flexibility, making them suitable for uneven surfaces. Their primary function is thermal management; however, due to their compliant nature, they can also introduce a damping effect that reduces vibration transmission.

Stiffeners

Stiffners (Figure 1.13) are generally transversal plates placed on the board which increase the stiffness of the PCA and ensure that the board remains flat under mechanical stresses.

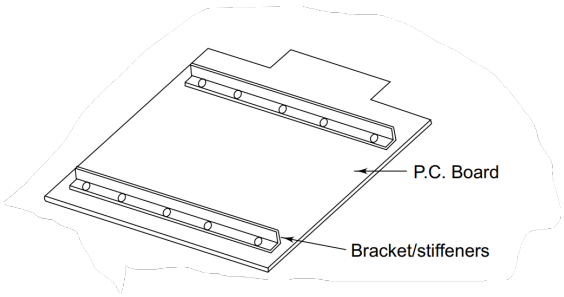

Figure 1.13: Use of stiffners on PCBs

1.2 Vibrations

Any motion that repeats itself after an interval of time is called vibration or oscillation. The theory of vibration deals with the study of oscillatory motions of bodies and the forces associated with them [6]. A vibratory system, in general, includes a means for storing potential energy (spring or elasticity), a means for storing kinetic energy (mass or inertia), and a means by which energy is gradually lost (damper).

The minimum number of independent coordinates required to determine completely the positions of all parts of a system at any instant of time defines the number of degrees of freedom of the system. Systems with a finite number of degrees of freedom are called discrete or lumped parameter systems, and those with an infinite number of degrees of freedom are called continuous or distributed systems.

1.2.1 Classification of Vibration

Vibration can be classified in several ways. Some of the important classifications are as follows [6].

Free and Forced Vibration If a system, after an initial disturbance, is left to vibrate on its own, the ensuing vibration is known as free vibration. No external force acts on the system. If a system is subjected to an external force (often, a repeating type of force), the resulting vibration is known as forced vibration. If the frequency of the external force coincides with one of the natural frequencies of the system, a condition known as resonance occurs, and the system undergoes dangerously large oscillations. Failures of structures have been associated with the occurrence of resonance.

Undamped and Damped Vibration If no energy is lost or dissipated in friction or other resistance during oscillation, the vibration is known as undamped vibration. If any energy is lost in this way, however, it is called damped vibration. In many physical systems, the amount of damping is so small that it can be disregarded for most engineering purposes.

Deterministic and Random Vibration If the value or magnitude of the excitation (force or motion) acting on a vibratory system is known at any given time, the excitation is called deterministic. The resulting vibration is known as deterministic vibration. In practice purely deterministic vibrations are only theoretical, physical systems are generally subjected to a combination of deterministic and random excitations. For nondeterministic or random excitations, the value of the excitation

at a given time cannot be predicted. In these cases, a large collection of records of the excitation may exhibit some statistical regularity. It is possible to estimate averages such as the mean and mean square values of the excitation.

1.2.2 Harmonic motion

Oscillatory motion may repeat itself regularly. If the motion is repeated after equal intervals of time, it is called periodic motion. The simplest type of periodic motion is harmonic motion (Figure 1.14).

The following definitions and terminology are useful in dealing with harmonic motion and other periodic functions [6].

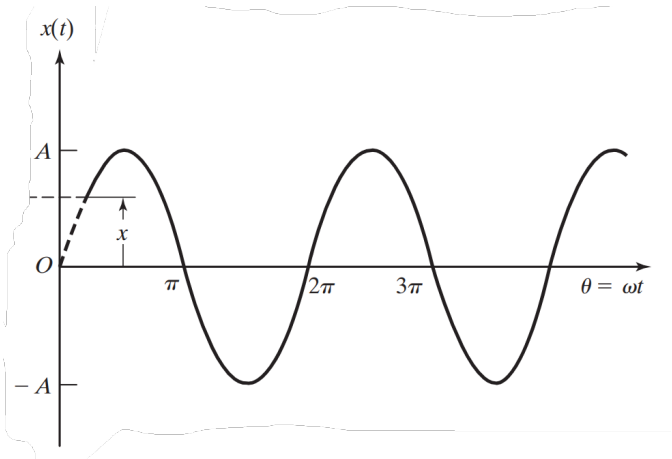

Figure 1.14: Harmonic motion 2D rapresentation [6]

Cycle The movement of a vibrating body from its undisturbed or equilibrium position to its extreme position in one direction, then to the equilibrium position, then to its extreme position in the other direction, and back to equilibrium position is called a cycle of vibration.

Amplitude The maximum displacement of a vibrating body from its equilibrium position is called the amplitude of vibration.

Period of oscillation The time taken to complete one cycle of motion is known as the period of oscillation or time period and is denoted by

$$T = \frac{2\pi}{\omega}$$

where ω is called the circular frequency.

Frequency of oscillation The number of cycles per unit time is called the frequency of oscillation or simply the frequency and is denoted by f. Thus

$$f = \frac{1}{T} = \frac{\omega}{2\pi}$$

Mode of vibration A mode of vibration can be defined as a way of vibrating, or a pattern of vibration, when applied to a system or structure that has several points with different amplitudes of deflection. A mode of vibration comprises two distinct elements: first, a time variation of the vibration and, second, a spatial variation of the amplitude of the motion across the structure. The time variation defines the frequency of oscillations together with any associated rate of decay or growth. The spatial variation defines the different vibration amplitudes from one point on the structure to the next.

Natural frequency If a system, after an initial disturbance, is left to vibrate on its own, the frequency with which it oscillates without external forces is known as its natural frequency. A vibratory system having n degrees of freedom will have, in general, n distinct natural frequencies of vibration. The first harmonic mode of a system, with the lowest natural frequency, is the fundamental resonant mode; this often has the greatest displacement amplitudes and usually the greatest stresses.

Mode shape It is a dimensionless shape function defined over the space of a structure that describes the relative displacement of any point as the structure vibrates in a single mode. There is a unique mode shape for each natural frequency of the structure [7].

1.3 Case Study

The type of PCA analyzed in this thesis represents a narrow category. In particular two real Electronic Control Units (ECUs), produced and validated by Marelli S.p.A., having similar characteristics were selected as case study.

In Figure 1.15 the exploded view of an example of this type of ECU is presented. Each assembly is composed of multiple parallel printed circuit boards, shown in green, which are electrically interconnected by vertically oriented board-to-board connectors. In addition, the boards are connected through perpendicular connectors to a smaller board, also shown in green. The perpendicular board hosts the external connectors and provides the interface with the external environment. The mechanical connection between the boards and to the external box and the cover is provided by the spacers or standoffs.

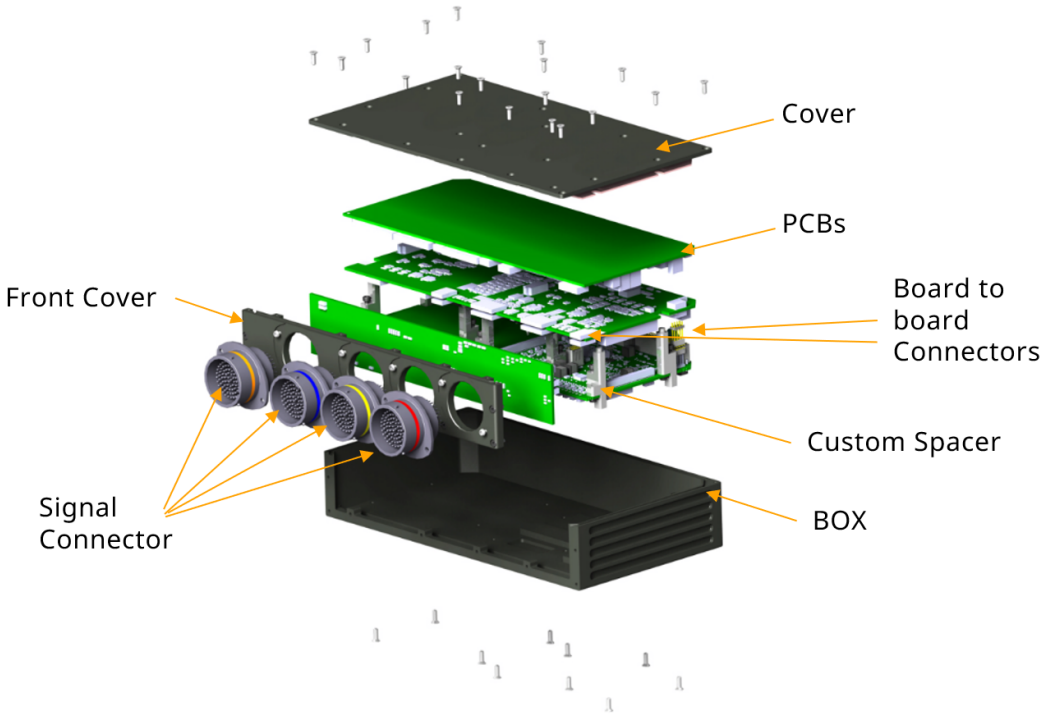

Figure 1.15: ECU Mid-range Build up Elements example

The studied ECUs, referred to as ECU-1 (Figure 1.16) and ECU-2 (Figure 1.17), are characterized by two parallel boards and a perpendicular one. The average weight of these ECUs is about 1 kg.

All the PCBs are rigid multilayer boards made of copper and FR4. The boards are populated according to the functional scope of the assembly, which in this

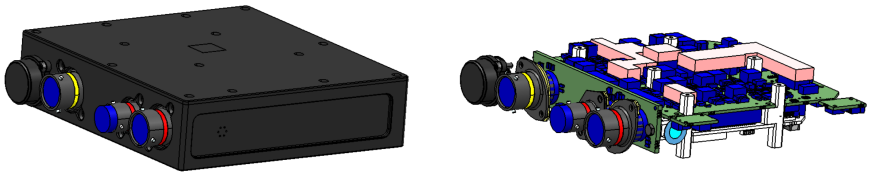

Figure 1.16: ECU-1 CAD representation. With case (left) and without (right)

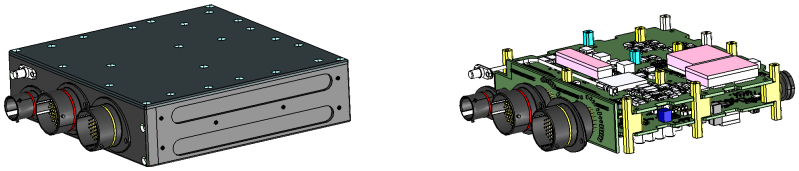

Figure 1.17: ECU-2 CAD representation. With case (left) and without (right)

case is data processing for motorsport applications. As a result, they are densely populated, predominantly with small components, complemented by a limited number of larger surface-mounted devices. To improve thermal dissipation, thermal pads are included, as shown in Figure 1.16 and 1.17 (highlighted in pink).

Electronic assemblies employed in automotive applications are required to withstand the vibration loads generated by their operating environment. The main excitation sources are the engine and the road induced vibrations transmitted through the chassis (Figure 1.18).

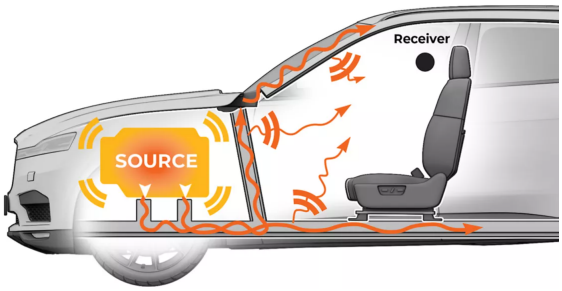

Figure 1.18: Engine vibration path

In motorsport, these assemblies are subjected to particularly demanding vibrational conditions, both in terms of frequency content and load intensity. To ensure product reliability, systems must undergo rigorous qualification before being released to the customer. Marelli S.p.A. (BU Motorsport) has established an internal guideline that specifies the functional vibration tests to be performed on

each electronic assembly.

The verification procedure consists of three main steps. First, a sinusoidal sweep test is carried out up to 2000 Hz to identify the resonant frequencies of the Device Under Test (DUT). Then, a random vibration fatigue test is conducted to reproduce the operational loads expected throughout the lifetime of the product. The profile of this random test depends on the intended mounting location: for example, devices installed in the engine compartment are exposed to higher excitation levels compared to units located in less severe areas of the vehicle, such as the cockpit. Accordingly, their Power Spectral Density (PSD) levels are defined more stringently. Finally, mechanical shock testing is performed. To guarantee repeatability and reproducibility, the half-sine pulse shape has been standardized as the excitation waveform. Similarly to random vibration, the severity of the shock test is adapted to the specific application class of the device.

Throughout all qualification steps, strict acceptance criteria apply. The DUT must not exhibit mechanical damage, functional or performance degradation, intermittent behavior, or undesired operation. Furthermore, no signs of physical deformation are tolerated at the end of the test.

1.4 Goal

The goal of this thesis is to provide a structured design guideline for selecting the number and placement of supports in PCAs. The aim is to make this choice more objective and quantitatively grounded, ensuring that the resulting assemblies can effectively withstand the high vibration levels typical of motorsport environments and successfully pass internal validation tests.

The fundamental frequency is used as the reference parameter as the highest deformations comes at the first natural frequency. Therefore functioning PCAs are experimentally investigated to understand their fundamental frequency and have an approximate reference value that guarantee good design.

Since during the design phase there is no physical model to test it is necessary to build a model that represent with preliminary info, available in design phase, the assembly to be designed. To define a proper model the fundamental frequency of the tested assemblies is compared to the one of the same assemblies computed via FEM adopting different models. Comparing the result of the experiment with the results of the FEM models the best trade off between simplicity of the model and accuracy is found.

Once a reliable modeling approach is defined, it can be used to perform a systematic study on the influence of the number and placement of supports on the first natural frequency of the PCA. By simulating different configurations, it becomes possible to identify the support layouts that maximize the fundamental

frequency.

The final objective is to establish a set of optimized support configurations, each characterized by a dimensionless parameter λ that relates the geometry and boundary conditions of the board to its natural frequency. These configurations can then serve as a reference during the design phase: knowing the desired first natural frequency and the basic physical properties of the PCA, designers can estimate the most suitable support layout without the need for time consuming simulations.

Chapter 2

Experimental Tests

In this chapter the available PCAs are experimentally investigated with the aim of identifying a pattern on the first natural frequency that guarantee proper functioning of the PCA. The tests are carried out separately for each PCA.

2.1 Instrumentation and setup

The tests are preformed on a shaker (V875-240 LDS) configured to impose a sine sweep vibration ranging from 30 to 2000 Hz with an acceleration amplitude of 2 g. The control of the shaker is managed through two control accelerometers (DYTRAN TRIAX 3033B2) shown in Figure 2.2a, with their average acceleration used as the feedback signal to maintain the target level (Figure 2.1).

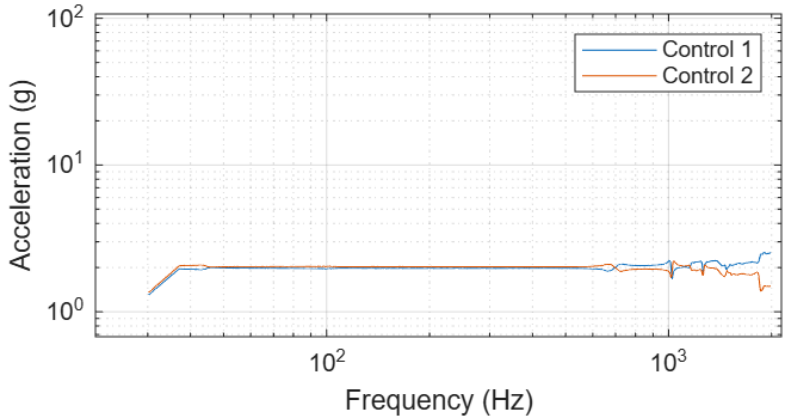

Figure 2.1: Control signal corresponding to a sine sweep of 2 g

The Device Under Test (DUT) is then mounted on the shaker, and additional accelerometers (DYTRAN 3225F1) shown in Figure 2.2b are used to monitor the

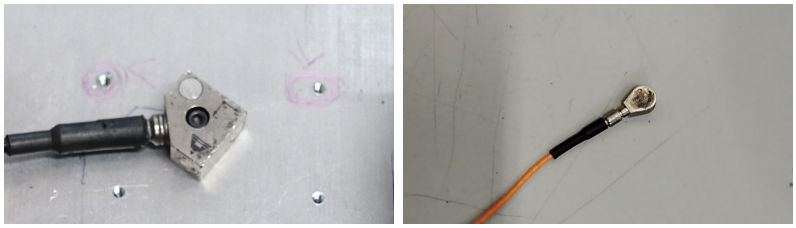

(a) Triaxial accelerometer **(b)** Monoaxial accelerometer

Figure 2.2: Accelerometers

acceleration response of the DUT at selected locations.

The DUT is mounted through standoffs on an adapter plate, which is firmly bolted to the shaker through the head expander. The control accelerometers are mounted through screws on the adapter plate, while the monitoring accelerometers are secured to the board using wax (Figure 2.3 and Figure 2.4).

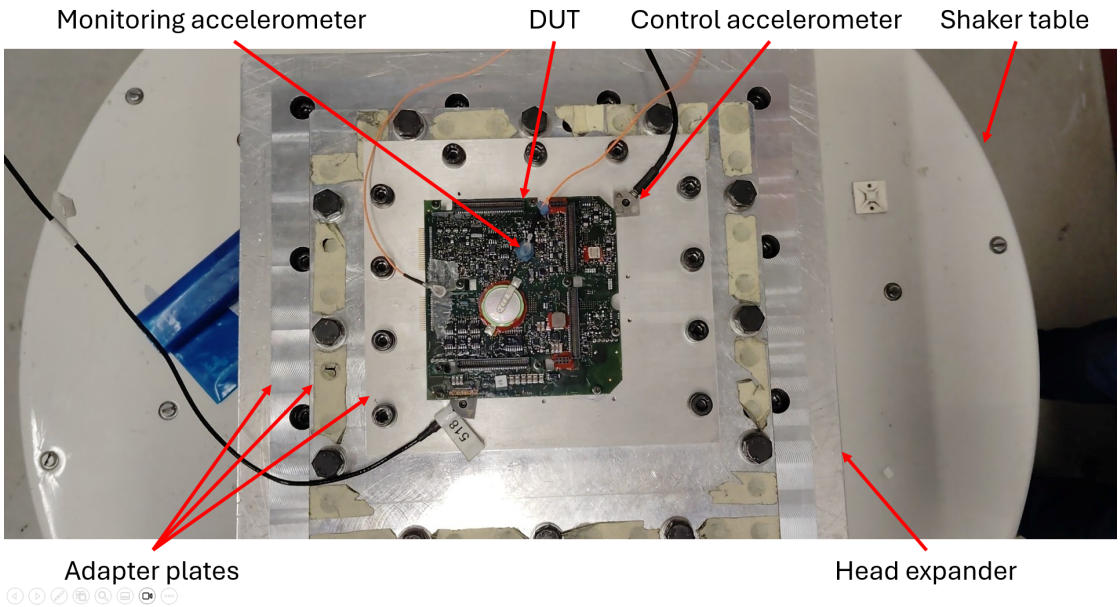

Figure 2.3: Shaker setup top view

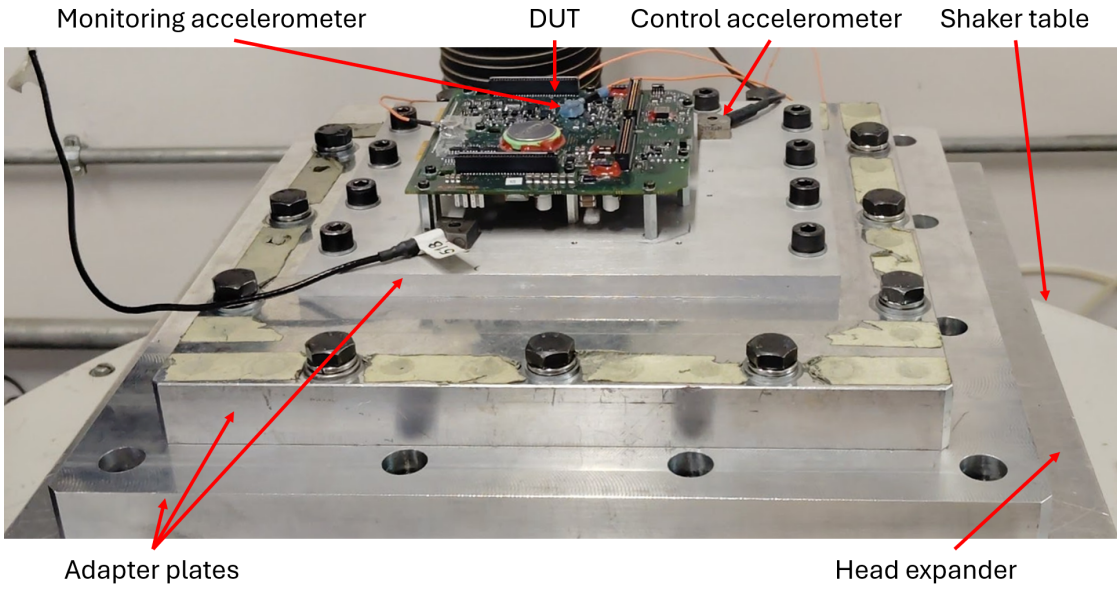

Figure 2.4: Shaker setup front view

The tested PCAs are:

- Board 1 (ECU-1) (Figure 2.5a)
- Board 2 (ECU-1) (Figure 2.5b)
- Board 3 (ECU-2) (Figure 2.5c)
- Board 4 (ECU-2) (Figure 2.5d)

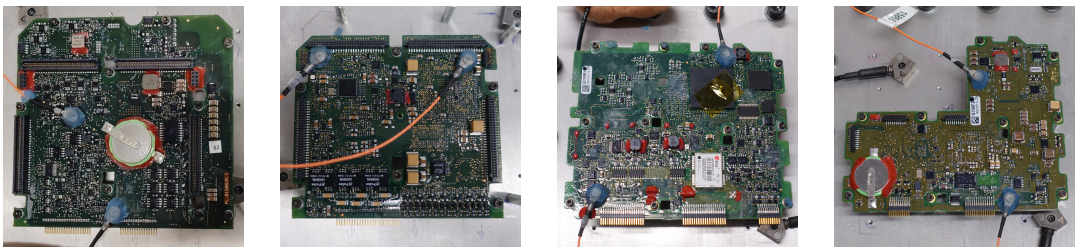

(a) Board 1 (ECU-1) **(b)** Board 2 (ECU-1) **(c)** Board 3 (ECU-2) **(d)** Board 4 (ECU-2)

Figure 2.5: Tested PCAs

2.2 Results

The output of the tests is the acceleration detected by each accelerometer in the interval of frequency from 30 to 2000 Hz.

2.2.1 Board 1

For Board 1, eight tests were performed changing the position of the two monitoring accelerometers. The sensor configurations are shown in Figure 2.6.

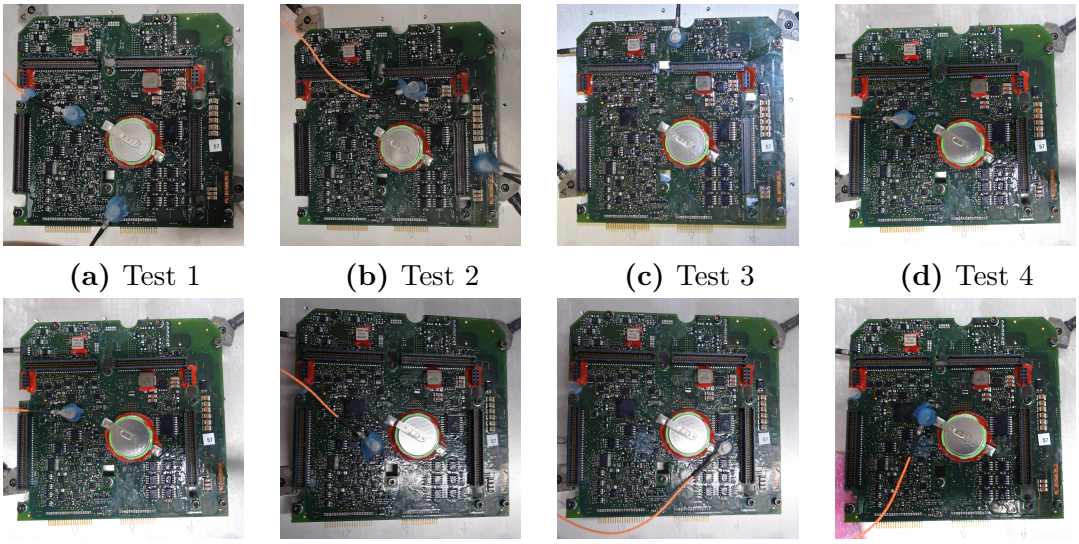

(a) Test 1 **(b)** Test 2 **(c)** Test 3 **(d)** Test 4

(e) Test 5 **(f)** Test 6 **(g)** Test 7 **(h)** Test 8

Figure 2.6: Accelerometers position during the tests performed on the Board 1

The corresponding Frequency Response Function (FRF) obtained from the two accelerometers in each test are shown in Figure 2.7 in logarithmic scale.

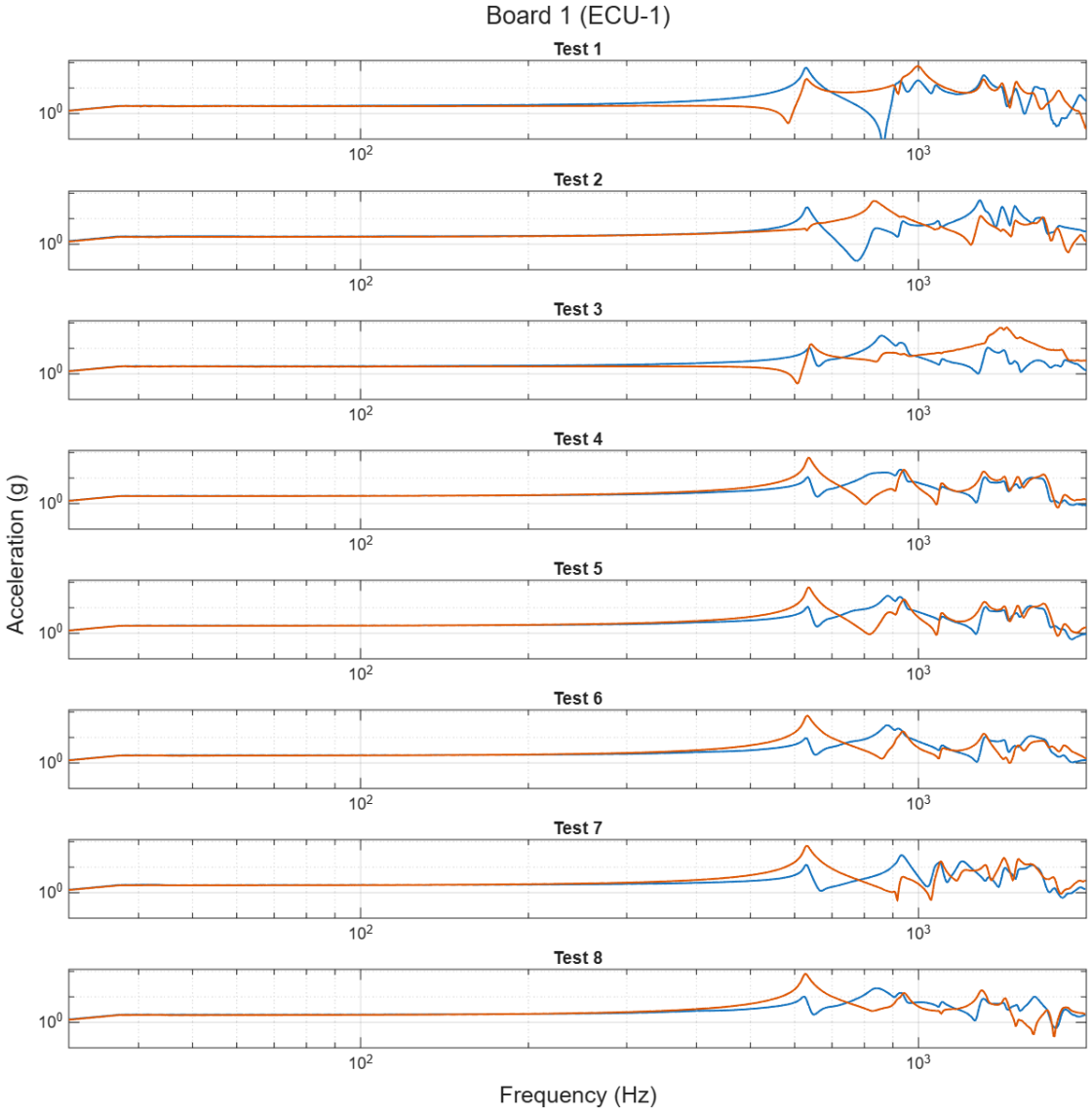

Figure 2.7: Frequency response functions of the monitoring accelerometers for all configurations of Board 1 (logarithmic scale)

Figure 2.8 highlights the resonance peaks identified for each signal. A consistent first natural frequency was observed between 600 and 700 Hz across all test configurations. For higher order modes, however, the responses varied significantly between configurations, with resonance peaks shifting depending on the accelerometer positions. This variation is attributed to the added mass of the accelerometers, which locally alters the dynamic response of the board.

From the eight tests performed on Board 1, the first natural frequency can be

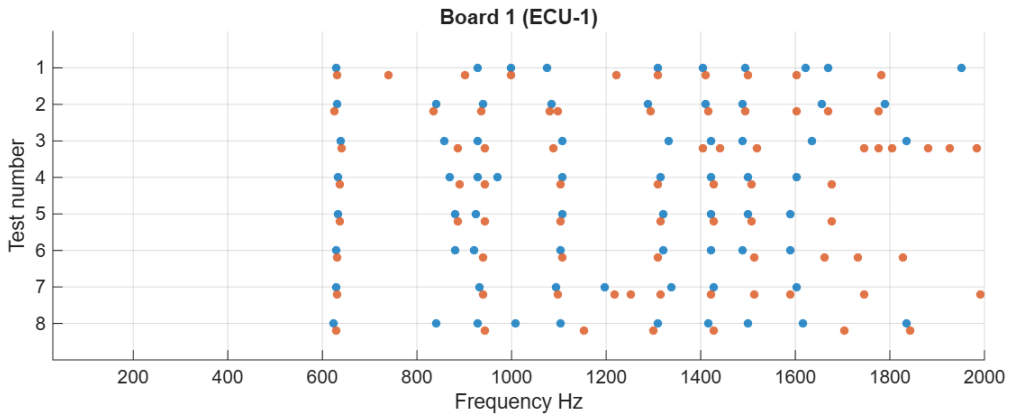

Figure 2.8: Resonance peaks identified for Board 1 in all test configurations (linear scale)

characterized by a mean value of 632 Hz with a Standard Deviation (SD) of 5 Hz, which correspond to a Coefficient of Variation (CV) lower then 1%.

2.2.2 Board 2

For Board 2, seven tests were conducted with different placements of the two monitoring accelerometers. The sensor configurations adopted in each test are illustrated in Figure 2.9.

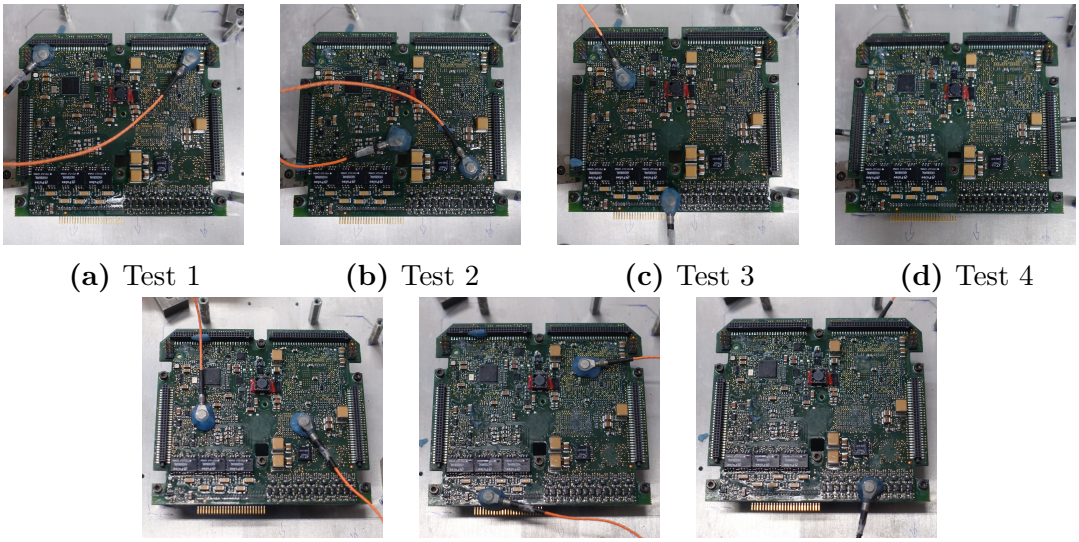

(a) Test 1 **(b)** Test 2 **(c)** Test 3 **(d)** Test 4

(e) Test 5 **(f)** Test 6 **(g)** Test 7

Figure 2.9: Accelerometers position during the tests performed on the Board 2

The corresponding FRFs are shown in Figure 2.10, reported in logarithmic scale.

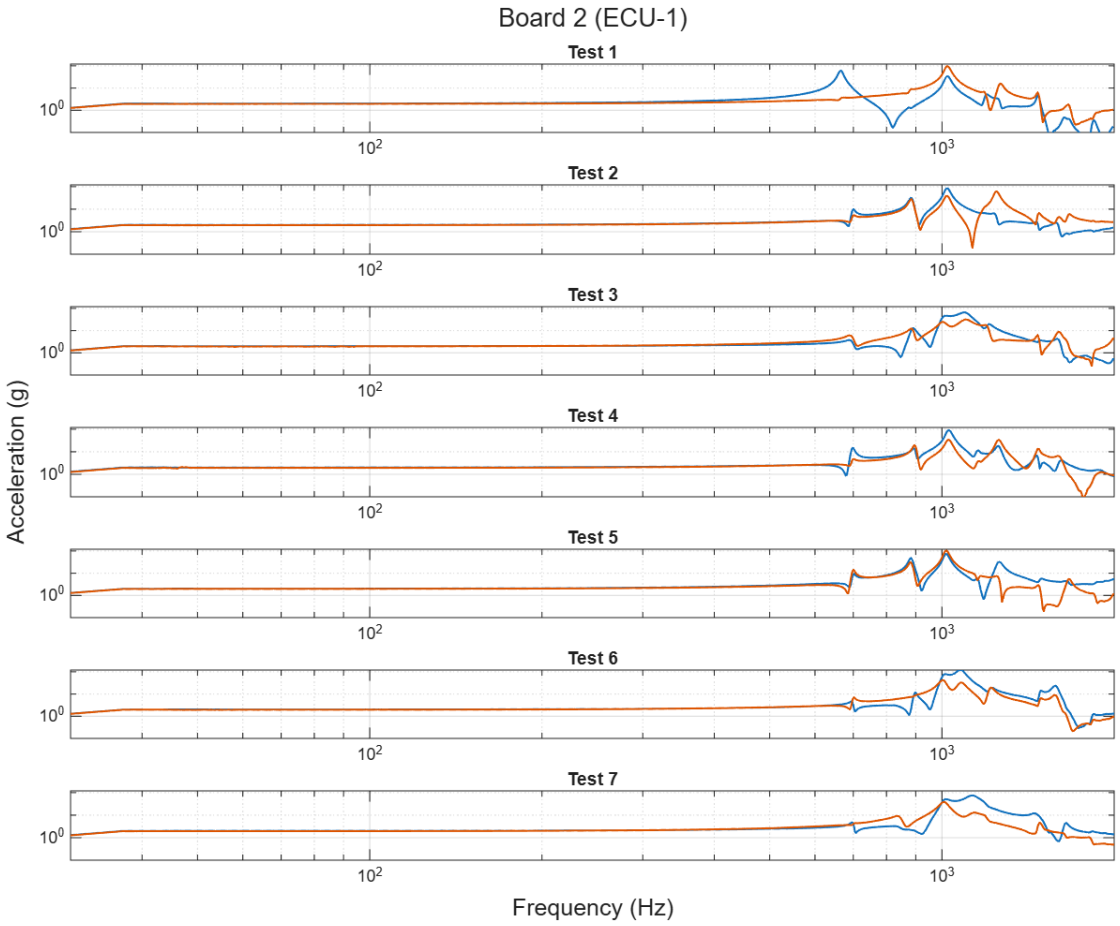

Figure 2.10: Frequency response functions of the monitoring accelerometers for all configurations of Board 2 (logarithmic scale)

The resonance peaks identified from each configuration are summarized in Figure 2.11. A first natural frequency was consistently observed around 600 and 700 Hz, although the spread among configurations was greater compared to Board 1.

From the statistical analysis of the seven tests, the first natural frequency of Board 2 can be described by a mean value of 681 Hz with a SD of 21 Hz, corresponding to a CV of approximately 3.1%.

2.2.3 Board 3

For Board 3, six tests were performed with different accelerometer placements, as illustrated in Figure 2.12.

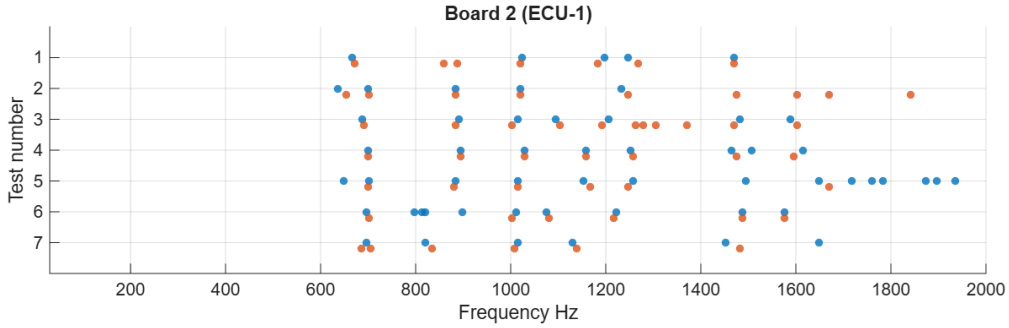

Figure 2.11: Resonance peaks identified for Board 2 in all test configurations (linear scale)

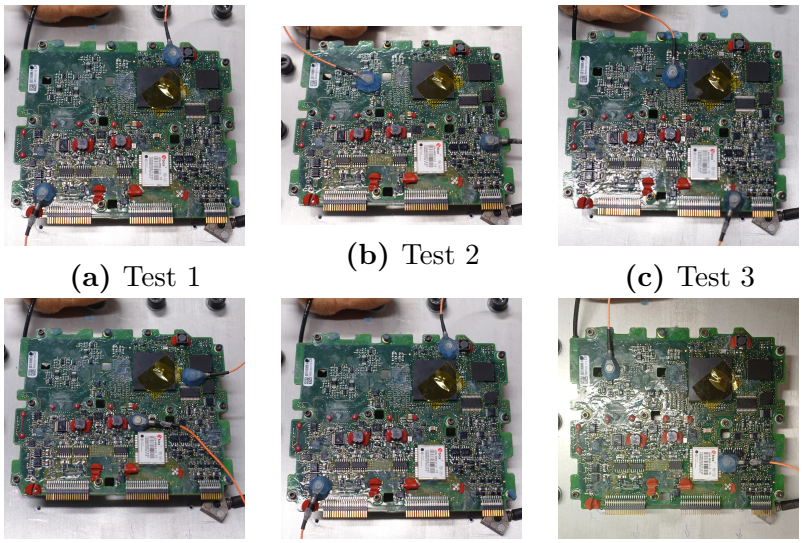

(a) Test 1 **(b)** Test 2 **(c)** Test 3

(d) Test 4 **(e)** Test 5 **(f)** Test 6

Figure 2.12: Accelerometers position during the tests performed on the Board 3

The resulting FRFs are reported in Figure 2.13 in logarithmic scale.

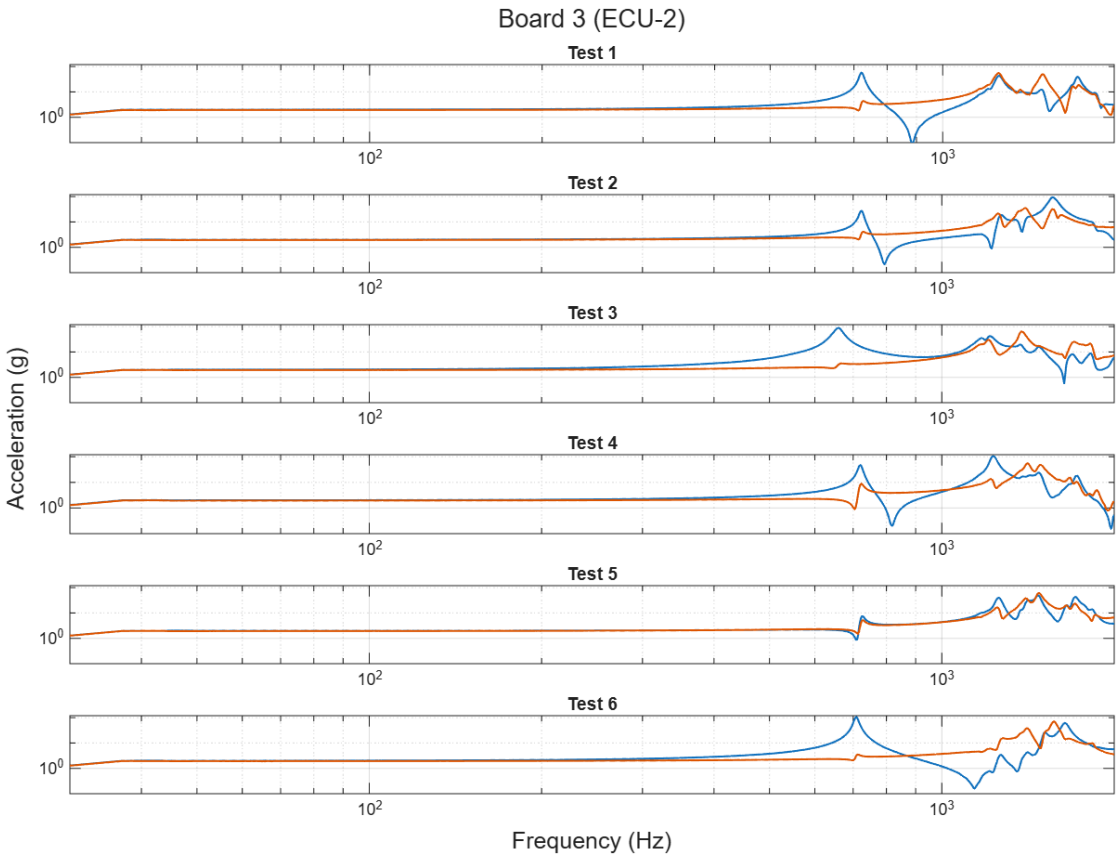

Figure 2.13: Frequency response functions of the monitoring accelerometers for all configurations of Board 3 (logarithmic scale)

The resonance peaks extracted from each configuration are shown in Figure 2.14. A first natural frequency was found around 700 Hz for all configurations, with a slightly higher value compared to Boards 1 and 2.

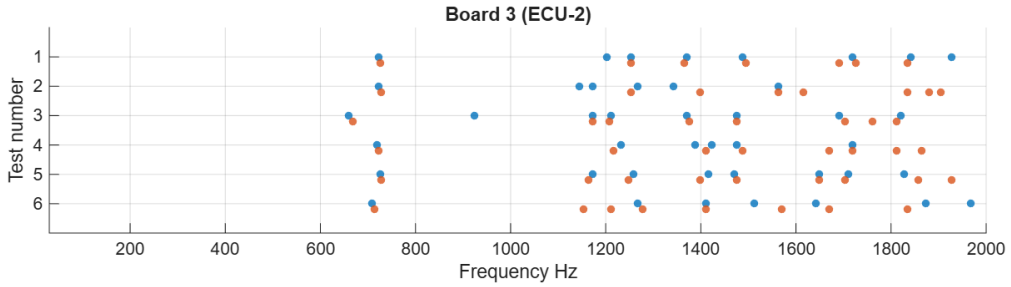

Figure 2.14: Resonance peaks identified for Board 3 in all test configurations (linear scale)

From the statistical analysis, the first natural frequency of Board 3 was found to have a mean value of 712 Hz with a SD of 23 Hz, corresponding to a CV of approximately 3.2%.

2.2.4 Board 4

For Board 4, six tests were conducted, and the accelerometer configurations are shown in Figure 2.15.

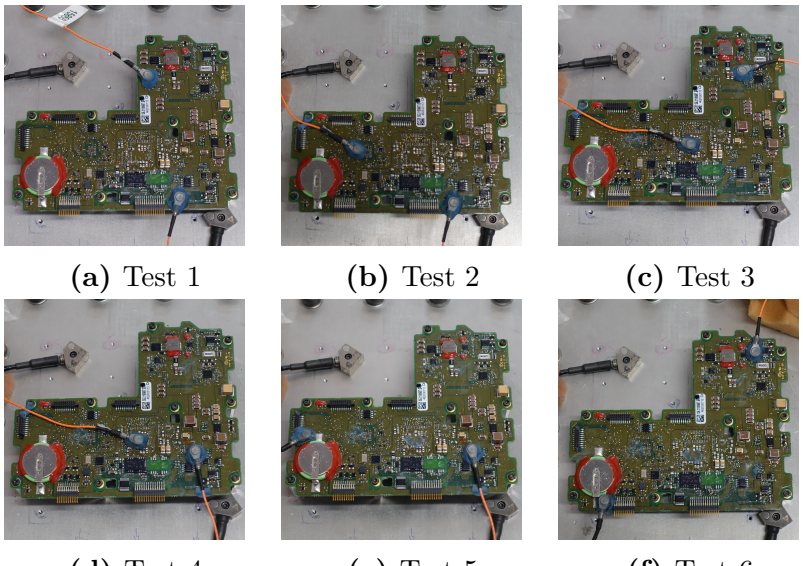

(a) Test 1 **(b)** Test 2 **(c)** Test 3

(d) Test 4 **(e)** Test 5 **(f)** Test 6

Figure 2.15: Accelerometers position during the tests performed on the Board 4

The corresponding FRF are shown in Figure 2.16 in logarithmic scale.

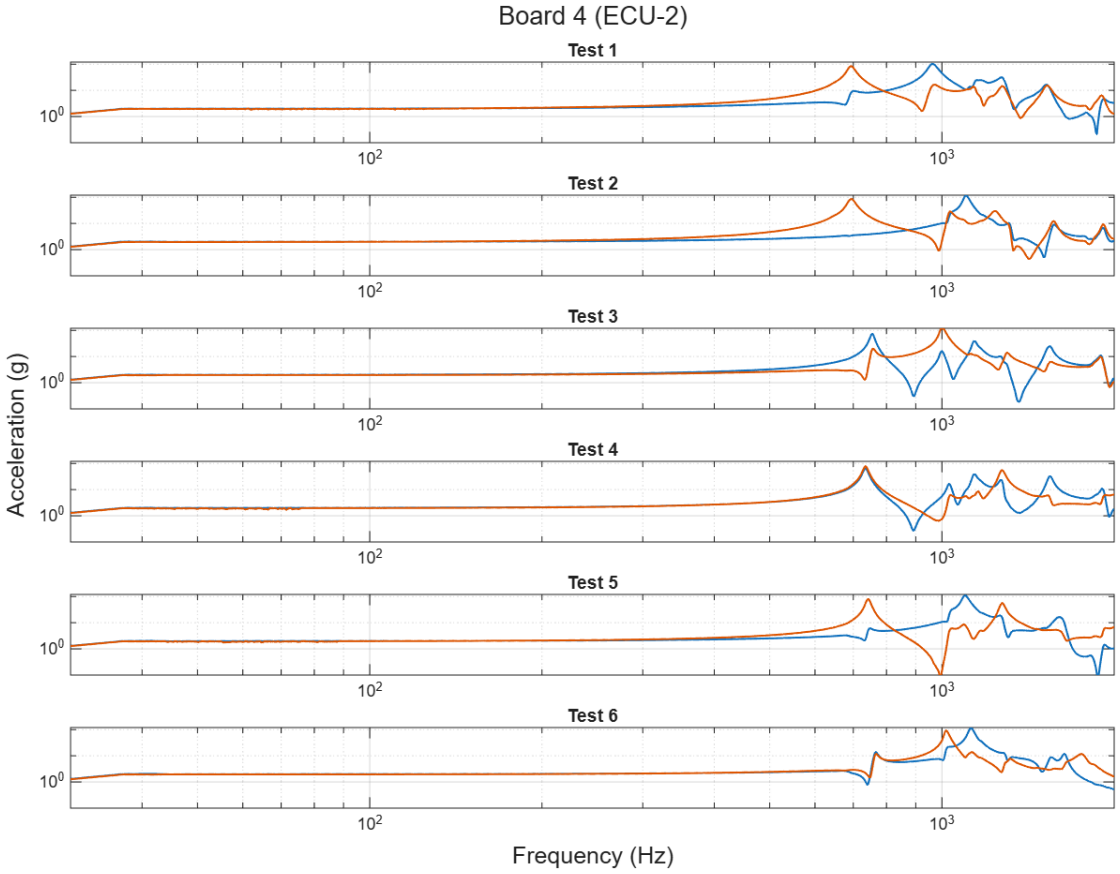

Figure 2.16: Frequency response functions of the monitoring accelerometers for all configurations of Board 4 (logarithmic scale)

The resonance peaks identified for each configuration are summarized in Figure 2.17. The first peak was observed around 700 Hz, similar to Board 3, although with greater variability among tests.

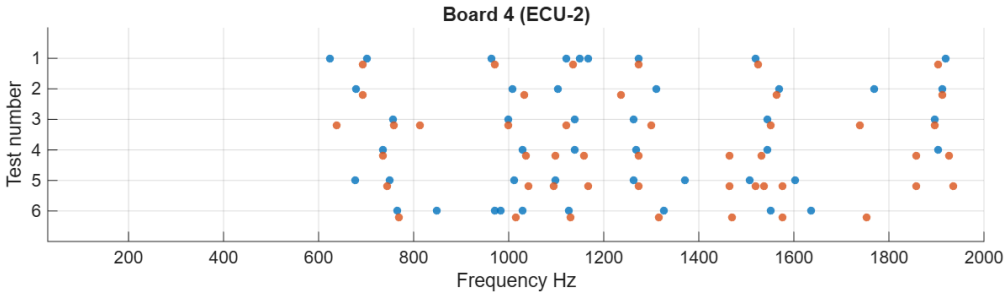

Figure 2.17: Resonance peaks identified for Board 4 in all test configurations (linear scale)

From the six tests conducted, the first natural frequency of Board 4 was found to have a mean value of 709 Hz with a SD of 49 Hz, corresponding to a CV of approximately 6.9%.

2.3 Conclusions

From the experimental campaign, it was found that all tested PCAs exhibit a similar first natural frequency (Figure 2.18), located approximately at 700 Hz, within a range between 600 and 800 Hz. This result is consistent across different board types and configurations, indicating that despite variations in geometry and component layout, the overall stiffness and support arrangement lead to comparable dynamic behavior.

A summary of the measured first natural frequencies for each board, together with the corresponding Standard Deviation (SD) and Coefficient of Variation (CV), is reported in Table 2.1. The limited dispersion of the first natural frequency among the tested assemblies suggests that this frequency range can be considered a reference value for properly designed and functioning PCAs. Assemblies exhibiting significantly lower fundamental frequencies are therefore expected to experience excessive deformation under vibration, potentially compromising functionality or reliability.

The experimental data obtained from these tests constitute the benchmark for the subsequent numerical analysis. In the following chapter, finite element models of the same assemblies are developed and correlated with the experimental results to assess their accuracy and identify a modeling approach suitable for early design validation.

BOARD	**1st PEAK [Hz]**	**SD [Hz]**	**CV**
1	632	5	0,8%
2	681	21	3,1%
3	712	23	3,2%
4	709	49	6,9%

Table 2.1: Summary of the first natural frequency, standard deviation, and coefficient of variation for each tested board

Figure 2.18: Resonance peaks identified for all the boards in all test configurations (linear scale)

Chapter 3

Printed Circuit Assembly Modeling and Simulation

In this chapter, the modeling approach adopted to estimate the fundamental frequency of PCA is presented.

The objective is to develop a simplified yet reliable FEM model that can be used during the early stages of the design process to support decisions regarding the number and placement of supports.

The FEM models developed in this work aim to reproduce the dynamic behavior of the experimentally tested assemblies using only the information typically available at the design stage, such as the board geometry, material properties, and support configuration. By comparing the natural frequencies obtained from experimental testing with those predicted by different FEM modeling strategies, the most suitable modeling approach is identified, balancing simplicity and accuracy.

3.1 State of Art

Before entering into the details of the present work, a brief review of the literature and relevant articles is presented.

3.1.1 Common Modeling Techniques

To obtain a reliable estimate of the dynamic behavior of a PCB, an appropriate modeling strategy must be selected. Pitarresi and Primavera [8] classified and evaluated the most common modeling techniques:

- **Simple Method:** The PCB is modeled as a homogeneous plate, neglecting the mass and stiffness contributions of the mounted components. The mechanical

Modeling Approach	Material Properties	Illustration
Simple Method	ρ_{PCB}, E_{PCB}, ν_{PCB} Components not modeled. Board is treated as homogeneous.	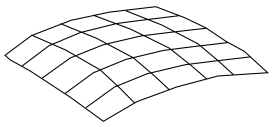
Global Mass Smearing	$\rho_{\text{PCB+components}}$, E_{PCB}, ν_{PCB} Total component mass is averaged into the board's density. Stiffness unchanged.	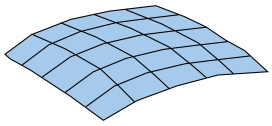
Global Mass/Stiffness Smearing	$\rho_{\text{PCB+components}}$, $E_{\text{PCB+components}}$, $\nu_{\text{PCB+components}}$ Both mass and stiffness contributions of components are averaged globally.	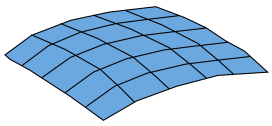
Local Smearing	Locally assigned: ρ_i, E_i, ν_i (based on component layout) Allows spatial variation of component effects over the PCB.	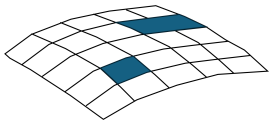
Detailed FE Model	Explicit modeling of components, solder joints, leads, and their geometry. Highest accuracy, highest computational cost.	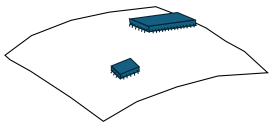

Table 3.1: Comparison of modeling strategies for PCB.

properties, Young's modulus E, density ρ, and Poisson's ratio ν, are assumed to be those of the unpopulated board, typically a mix of FR4 and copper.

- **Global Mass Smearing:** This approach extends the simple method by incorporating the total mass of the mounted components. An effective global density is computed by dividing the total mass by the board's volume. The increase in stiffness due to components is still neglected.

- **Global Mass/Stiffness Smearing:** Both mass and stiffness effects of the

components are considered. In addition to a global effective density, an effective global stiffness is introduced.

- **Local Smearing:** This technique applies the concept of smearing *locally*, assigning effective material properties, mass and stiffness, to specific regions of the board where components are located.

- **Detailed FE Model:** This method includes all mounted components, solder joints, and electrical leads explicitly. Although it yields the highest accuracy, the level of detail results in significant computational cost, making it impractical for most industrial applications.

The above techniques are summed up in Table 3.1.

The paper then presents a number of case studies in which experimental modal analysis results are compared with those obtained using the previously described modeling techniques.

The main finding is that a more complex model does not always guarantee a better representation of the actual dynamic behavior. Instead, the accuracy of the model depends strongly on the specific characteristics of the PCB. For certain applications, accounting only for the additional mass of the components, while neglecting their contribution to stiffness, can lead to significant deviations from experimental results.

3.1.2 Impact of PCA Application

The matter of determining the appropriate level of model simplification is then explored by Amy et al. [9], who propose a methodology to evaluate the accuracy of simplified finite element models of PCB under vibrational loading. The study focused on simplifying three properties of the system: mass, bending stiffness, and torsional stiffness. For each PCB configuration, a locally smeared "benchmark" model was generated, and a series of simplified models were created by modifying this reference case. Two types of simplification were considered: averaging, where component properties were redistributed (smeared) across the board, and neglecting, where component effects were entirely ignored. Each property (mass, stiffness, torsional stiffness) could be either averaged or neglected, resulting in multiple combinations of simplification types.

The global smearing process was performed in a way that conserved the total mass and stiffness of the system by weighting the component contributions by their area. In contrast, in the "neglected" case, component properties were simply excluded from the model. The simulations were repeated across a wide range of randomly generated PCB configurations. Table 3.2 summarizes the bare PCB variables considered in the analysis.

Variable	**Range**	**Distribution**
Thickness	1.6 or 2 mm	Discrete
Edge length	75-150 mm	Discrete (5 mm intervals)
Edge ratio	0.7-1.0	Continuous
Young's modulus	25.5×10^9 Pa	Constant
Density	1900 kg/m^3	Constant
Component areal density	0.1-0.5	Continuous

Table 3.2: Range and distribution of PCB parameters

Components were categorized into three groups (light, SMT, and heavy) based on their size and corresponding influence on the local mechanical properties. Table 3.3 lists the stiffness, and density multipliers associated with each category.

Component Type	**Edge Length [mm]**	**Stiffness Ratio**	**Density Ratio**
Light	5–10	1.3–1.6	1.5–2
SMT	10–30	1.33–3.5	1.5–6
Heavy	20–35	3–4	6–56

Table 3.3: Component classification based on edge length and equivalent smeared property ratios.

Based on intended application, PCBs were grouped into four classes according to component layout:

1. **Power:** only heavy components.
2. **Power and Processing:** equal areas of heavy and SMT components.
3. **Processing:** only SMT components.
4. **Light Processing:** equal areas of SMT and light components.

For each application class, multiple board configurations were generated, assigning components randomly over the board area while respecting the specified component proportions.

The analysis revealed that for boards used in light processing, where only small and SMT components are mounted, a globally smeared model using only mass averaging produced results very close to the locally smeared benchmark. This indicates that in such scenarios, simplified modeling can offer accurate predictions with significantly reduced computational effort.

3.1.3 PCB properties determination

Venkat et al. [10] addressed the issue of estimating the Young's modulus of an unpopulated PCB. They compared experimental results with the analytical formulation originally proposed by Steinberg [11] for composite beams, extended to plates as:

$$E_{\mathrm{PCB}} = E_{\mathrm{FR4}} \left(\frac{V_{\mathrm{PCB}} - V_{\mathrm{Cu}}}{V_{\mathrm{PCB}}} \right) + E_{\mathrm{Cu}} \left(\frac{V_{\mathrm{Cu}}}{V_{\mathrm{PCB}}} \right) \tag{3.1}$$

where E_{FR4} and E_C are the Young's moduli of FR4 and copper, respectively, and V_{PCB} and V_C are the total volume of the board and the copper volume. The analytical estimation resulted in an error of only 1% compared to experimental data.

The study further investigated the estimation of the first natural frequency of a PCB supported by standoffs, comparing analytical, FE, and experimental methods. The analytical approach led to significant deviation (around 20%) due to the inability to model discrete bolt boundary conditions accurately. Conversely, the FEM approach showed good agreement with the experimental results, with an error of only 5.45%.

3.1.4 Boundary conditions

The modeling of point supports, such as fastening screws and standoffs, has been approached differently by various authors. Chen [12] modeled the supports by clamping the edges of the holes used for screw fastening. In his work, he also mentions that fastening screws are often represented as simple supports reinforced by weak rotational springs. This approach is adopted by Amy et al. [13], who proposed a model that allows rotation of the constrained nodes while assigning an appropriate rotational stiffness, maintaining zero translational displacement.

Arabi et al. [14] investigated the effect of different modeling comparing the natural frequencies of the same PCB constrained first by a realistic screw-nut model and then by assigning zero displacement to the nodes of circles representing the zones of fixation (Figure 3.1).

The first five natural frequencies were obtained for the two configurations, the difference between frequencies for each mode does not exceed 1%.

3.2 Modeling Approach

3.2.1 Simulation type

A modal analysis was performed to determine the natural frequencies of the PCAs. The objective of the analysis is to estimate the first natural frequency, used as

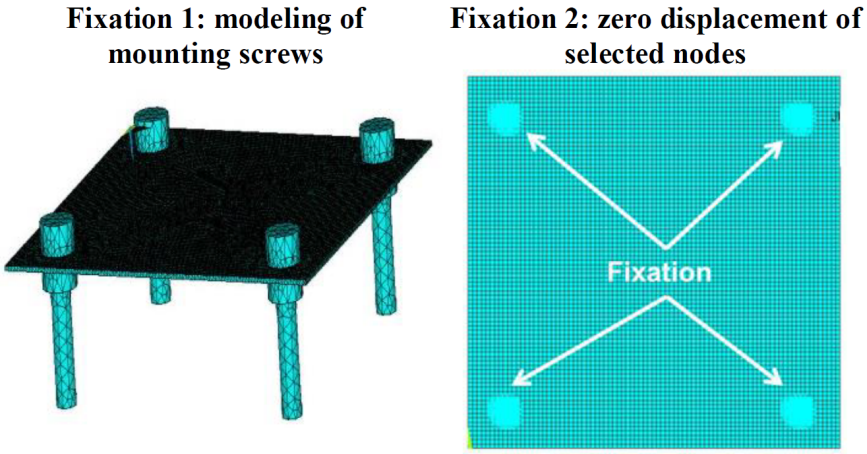

Figure 3.1: Modeling of PCB mounted through point supports [14]

reference parameter for evaluating the dynamic behavior of the assemblies.

The simulations were carried out in ANSYS Mechanical adopting a linear undamped analysis. This approach allows evaluating the dynamic properties of the structure independently from the excitation amplitude, assuming small deformations and linear elastic behavior. Damping effects were neglected since they mainly influence the vibration amplitude and not the natural frequency value.

3.2.2 Geometry and boundary conditions

A 2D geometry of the respective PCBs, discretized generating a program controlled mesh, was used for all the analysis (Figure 3.2). The nodes along the circumference of each mounting hole were constrained in translation, preventing any displacement while allowing free rotation.

3.2.3 Progressive Modeling

Here the models adopted for the PCAs dynamic simulations are presented. Since the modeling procedure is identical for all of them, the detailed workflow is illustrated only for one representative board, Board 1 of ECU-1. The results will be reported for all the tested PCAs.

Layer-Resolved PCB Model (D-N-N)

This model is characterized by a Detailed PCB model, Neglected components mass, and Neglected component stiffness, therefore will be also referred to as D-N-N.

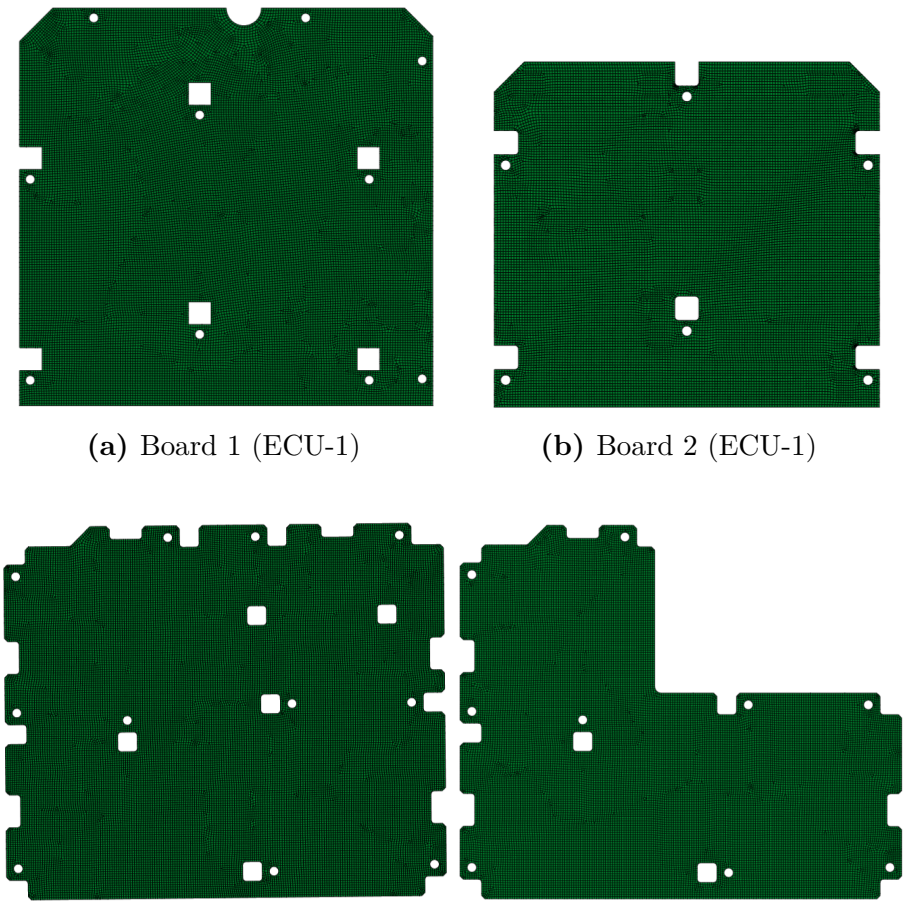

(a) Board 1 (ECU-1) **(b)** Board 2 (ECU-1)

(c) Board 3 (ECU-2) **(d)** Board 4 (ECU-2)

Figure 3.2: Geometry and mesh of the modeled boards

Unlike the "Simple Method" found in the literature, the PCB was not treated as a homogeneous plate. Instead, the multilayer structure was reconstructed directly from the available Electronic Computer Aided Design (ECAD) data (Figure 3.3), which provides the geometry of traces and vias together with the stack-up configuration.

Using the trace mapping feature of ANSYS, the copper fraction was assigned to each dielectric layer, allowing the creation of an equivalent representation of the PCB that takes into account the copper and FR4 distribution (Figure 3.4) without explicitly meshing the traces or vias. In this way, the main characteristics of the board composition were preserved while maintaining reasonable computational efficiency.

The model required as input the ECAD file of the PCB layout, the 2D geometry of the board, and the properties of the two base materials, FR4 and copper alloy.

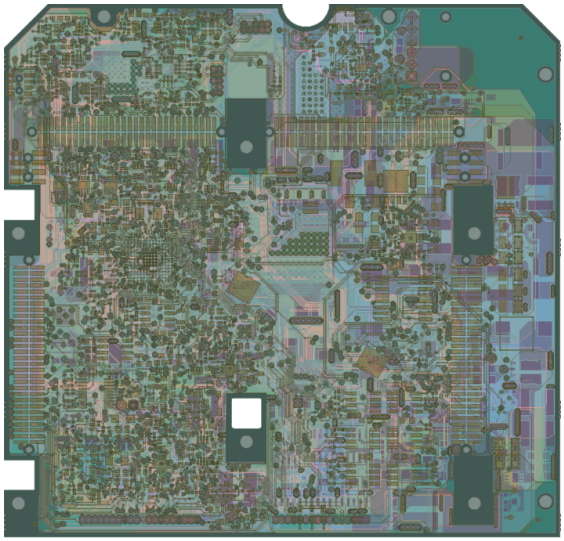

Figure 3.3: ECAD file, detailed layers of Board 1

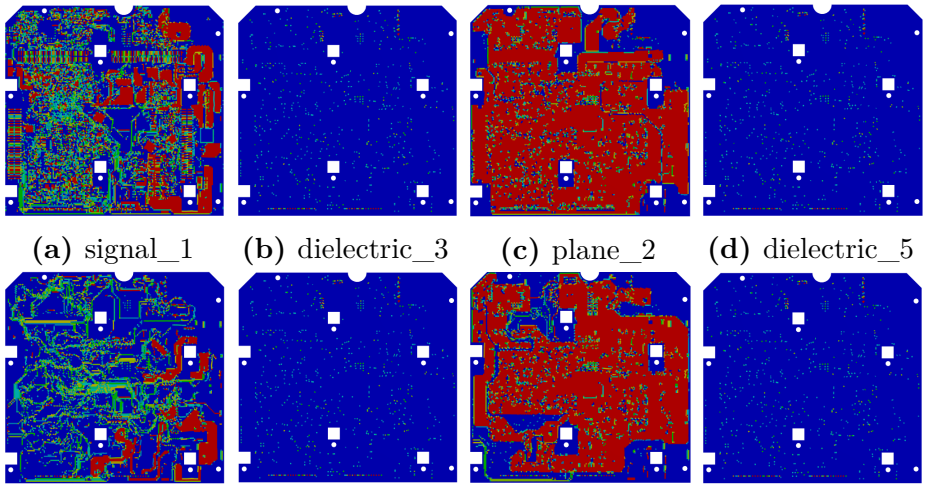

(a) signal_1 **(b)** dielectric_3 **(c)** plane_2 **(d)** dielectric_5

(e) signal_3 **(f)** dielectric_7 **(g)** plane_4 **(h)** dielectric_9

Figure 3.4: The first 8 (of 15) layers composing the PCB of Board 1. Each element of the mesh is assigned a percentage of copper. Red is 100%, blue is 0%.

The material properties adopted for the simulations are reported in Table 3.4. The copper properties were taken from the ANSYS library as they are well known and do not significantly vary between applications, while the FR4 properties were derived from the datasheet of the material typically employed by Marelli. When specific data for the FR4 used in the tested assemblies were not available, the missing parameters were approximated based on typical values for similar FR4

laminates.

Material	**Young's Modulus [GPa]**	**Poisson's Ratio**	**Density [kg/m^3]**
FR4	19.45	0.17	1850
Copper	110	0.34	8300

Table 3.4: D-N-N Model materials

From the ECAD import, the thickness of each layer and its copper fraction were extracted. Table 3.5 summarizes the main results.

Layer	**Thickness [mm]**	**Metal fraction [-]**
signal_1	0.017	0.3709
dielectric_3	0.100	0.0096
plane_2	0.035	0.7042
dielectric_5	0.200	0.0096
signal_3	0.035	0.2080
dielectric_7	0.200	0.0096
plane_4	0.035	0.6212
dielectric_9	0.300	0.0096
plane_5	0.035	0.6238
dielectric_11	0.200	0.0096
signal_6	0.035	0.3136
dielectric_13	0.200	0.0096
plane_7	0.035	0.8249
dielectric_15	0.100	0.0096
signal_8	0.017	0.4771
	Total thickness [mm] **1.54**	**Average Metal fraction [%]** **9.2**

Table 3.5: Layer properties of the PCB of Board 1

The trace-mapping procedure therefore provided, in addition to the effective material properties, the percentage of copper volume and the total thickness of the board.

The total t (thickness) of the PCB is computed as the sum of each layer thickness (Equation 3.2), while the average x_{Cu} (copper fraction) is computed as the average of the layers copper fraction weighted on each layer thickness (Equation 3.3).

$$t_{\mathrm{PCB}} = \sum_{i}^{n_{\mathrm{layers}}} t_i = 1.54 \text{ mm} \tag{3.2}$$

$$x_{\text{Cu,PCB}} = \sum_{i}^{n_{\text{layers}}} x_{Cu,i} \cdot t_i = 0.092 \tag{3.3}$$

This layer-resolved model is used in the following as a reference baseline for the subsequent FEM representations constituted by an homogeneous model of the PCB.

The natural frequencies of the model were computed up to 2000 Hz. The results are presented in Figure 3.5, where a horizontal line indicates the mean value of the first experimental resonance identified for Board 1.

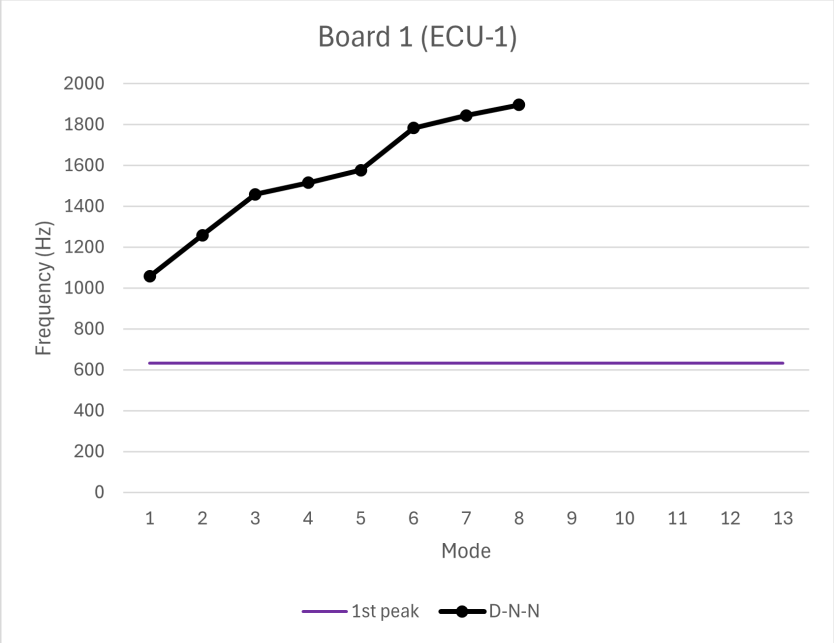

Figure 3.5: D-N-N modes up to 200 Hz of Board 1

The accuracy of the model is evaluated comparing the first natural frequency of the model with the mean frequency of the first peak of the experimental tests. As shown in Figure 3.6 the model shows great inaccuracy presenting the first mode at 1057 Hz, more then 60% higher then the first peak experimentally evaluated at about 632 Hz.

Simple Method A-N-N

This model is characterized by an Averaged PCB model, Neglected components mass, and Neglected component stiffness, therefore will be also referred to as A-N-N.

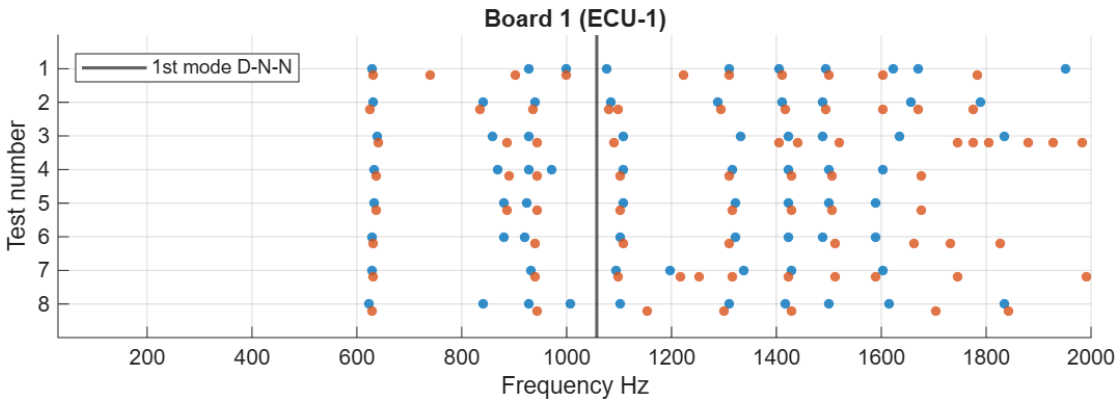

Figure 3.6: D-N-N 1st mode versus experimental peaks of Board 1

The PCA is modeled as a 2D surface characterized by the thickness computed in the previous model.

The properties of the material assigned to the surface are the average of the dielectric and trace materials properties (FR4 and copper) weighted on the respective volume. Equation 3.1 can then be rewritten as Equation 3.4.

$$E_{\text{PCB}} = E_{\text{FR4}} \cdot (1 - x_{\text{Cu,PCB}}) + E_{\text{Cu}} \cdot x_{\text{Cu,PCB}} = 27.8 \text{ GPa} \tag{3.4}$$

Similarly the ν (Poisson's ratio) and the ρ (density) are computed as follows.

$$\nu_{\text{PCB}} = \nu_{\text{FR4}} \cdot (1 - x_{\text{Cu,PCB}}) + \nu_{\text{Cu}} \cdot x_{\text{Cu,PCB}} = 0.186 \tag{3.5}$$

$$\rho_{\text{PCB}} = \rho_{\text{FR4}} \cdot (1 - x_{\text{Cu,PCB}}) + \rho_{\text{Cu}} \cdot x_{\text{Cu,PCB}} = 2440 \text{ kg/m}^3 \tag{3.6}$$

Material	**Young's Modulus [GPa]**	**Poisson's Ratio**	**Density [kg/m^3]**
PCB	27.8	0.186	2440

Table 3.6: A-N-N materials

In Figure 3.7 it is possible to observe that the natural frequencies of the new model are almost overlapping with the ones computed in the previous model. This result shows that the information lost in considering the PCB uniform is negligible.

The accuracy of the model is still very low, as shown in Figure 3.8, the first mode at 1073 Hz, still more then 60% higher then the first peak at about 632 Hz, is not representative of the real PCA.

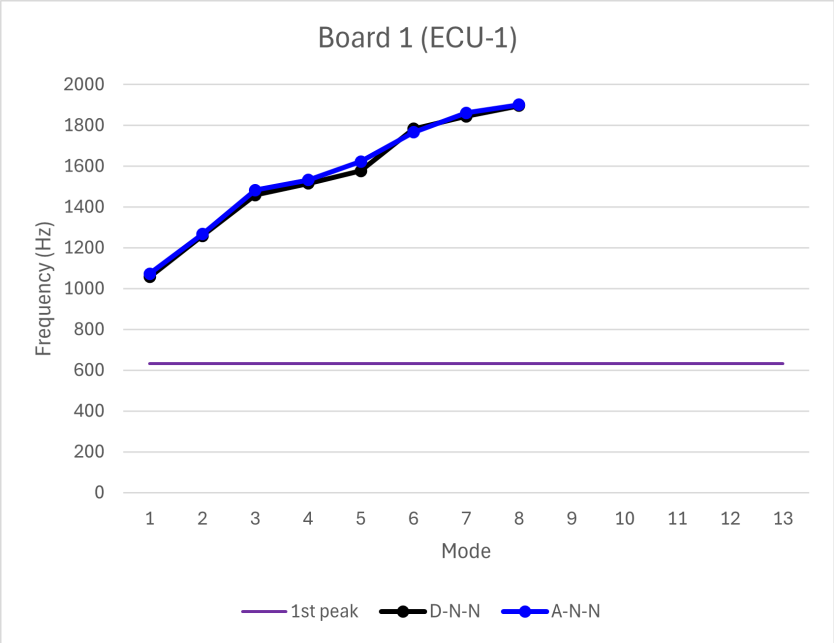

Figure 3.7: A-N-N modes up to 200 Hz of Board 1

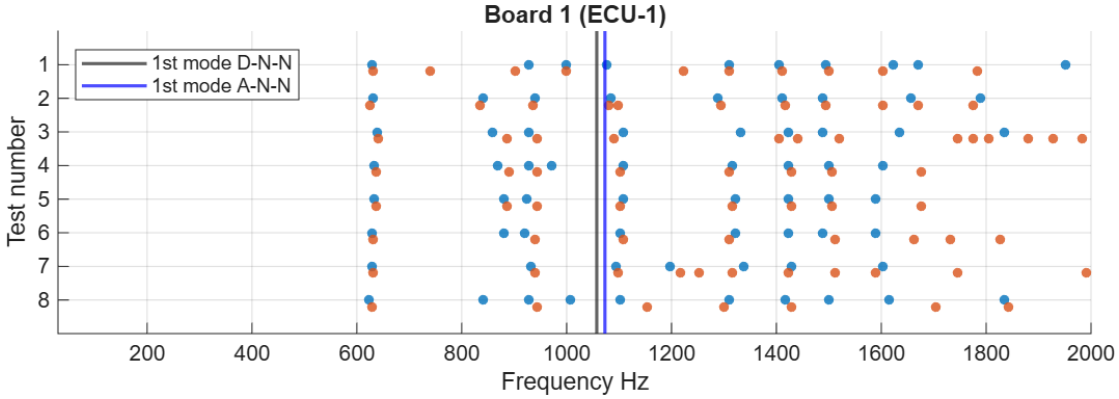

Figure 3.8: A-N-N 1st mode versus experimental peaks of Board 1

Global Mass Smearing A-A-N

This model is characterized by an Averaged PCB model, Averaged components mass, and Neglected component stiffness, therefore will be also referred to as A-A-N.

The real PCA m (mass) was then measured on a scale (Figure 3.9) and the density was computed as in Equation 3.7.

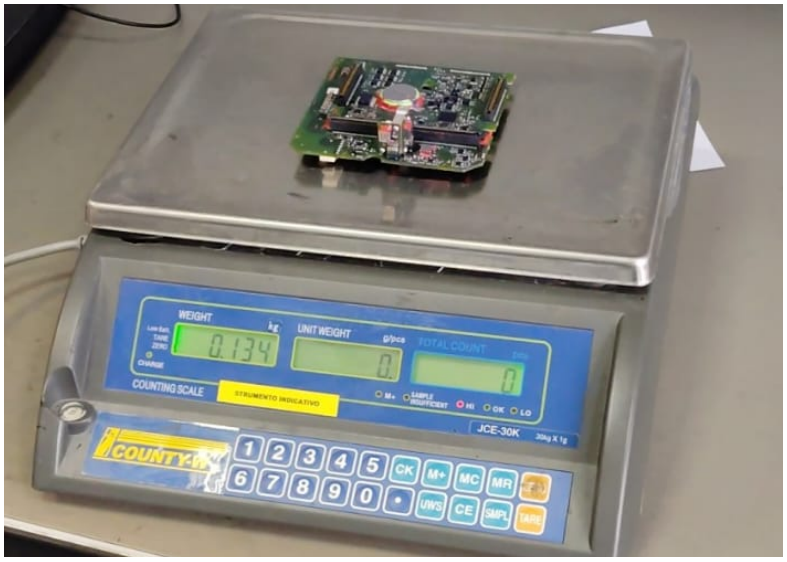

Figure 3.9: Caption

$$\rho_{\text{PCA'}} = \frac{m_{\text{PCA}}}{V_{\text{PCB}}} = 6800 \text{ kg/m}^3 \tag{3.7}$$

The properties are summed up in Table 3.7

Material	**Young's Modulus [GPa]**	**Poisson's Ratio**	**Density [kg/m^3]**
PCA'	27.8	0.186	6800

Table 3.7: A-A-N materials

The contribution of the components mass consistently shifted all the natural frequencies to lower values, presenting the first natural frequency to be really close to the one evaluated experimentally (Figure 3.10).

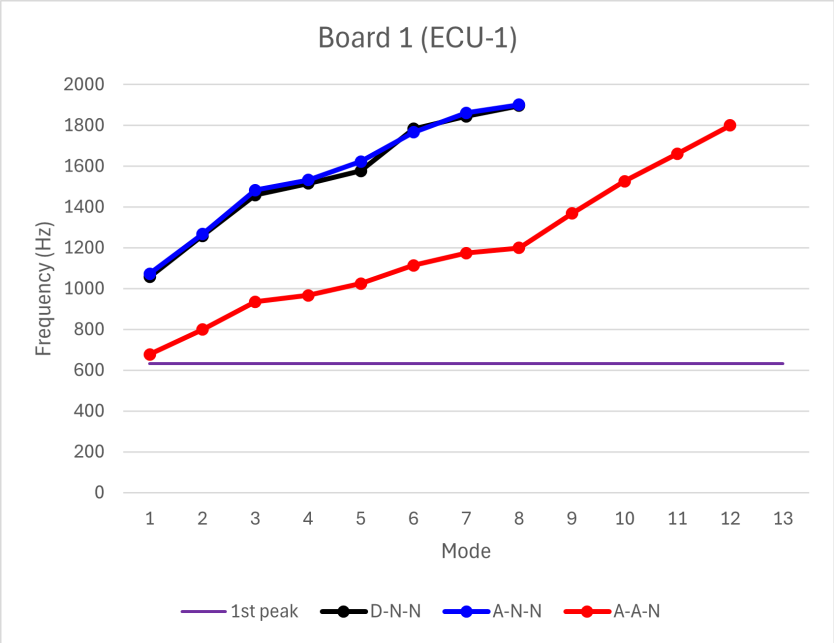

Figure 3.10: A-A-N modes up to 200 Hz of Board 1

The same behavior can be observed in Figure 3.11, the computed fundamental frequency at 677 Hz is only 7% higher then the experimental first peak at 632 Hz.

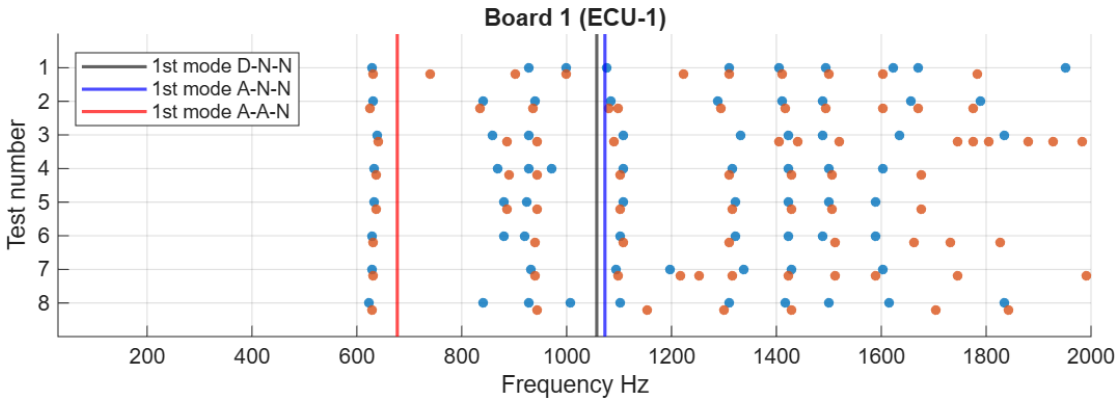

Figure 3.11: A-A-N 1st mode versus experimental peaks of Board 1

3.3 Results

The results already presented for Board 1 are presented here for all the assemblies.

Figure 3.12 shows the natural frequencies up to 2000 Hz obtained from the different finite element models. The D–N–N model (black) and the A–N–N model

(blue) exhibit only small variations in the predicted frequencies across the different boards, indicating that the information loss due to model simplification is limited. However, since these configurations neglect the contribution of the component masses, they are not suitable for accurately estimating the first natural frequency of the real PCA. The experimental reference value, corresponding to the mean of the first measured peaks, is indicated as a purple horizontal line. From Figure 3.12

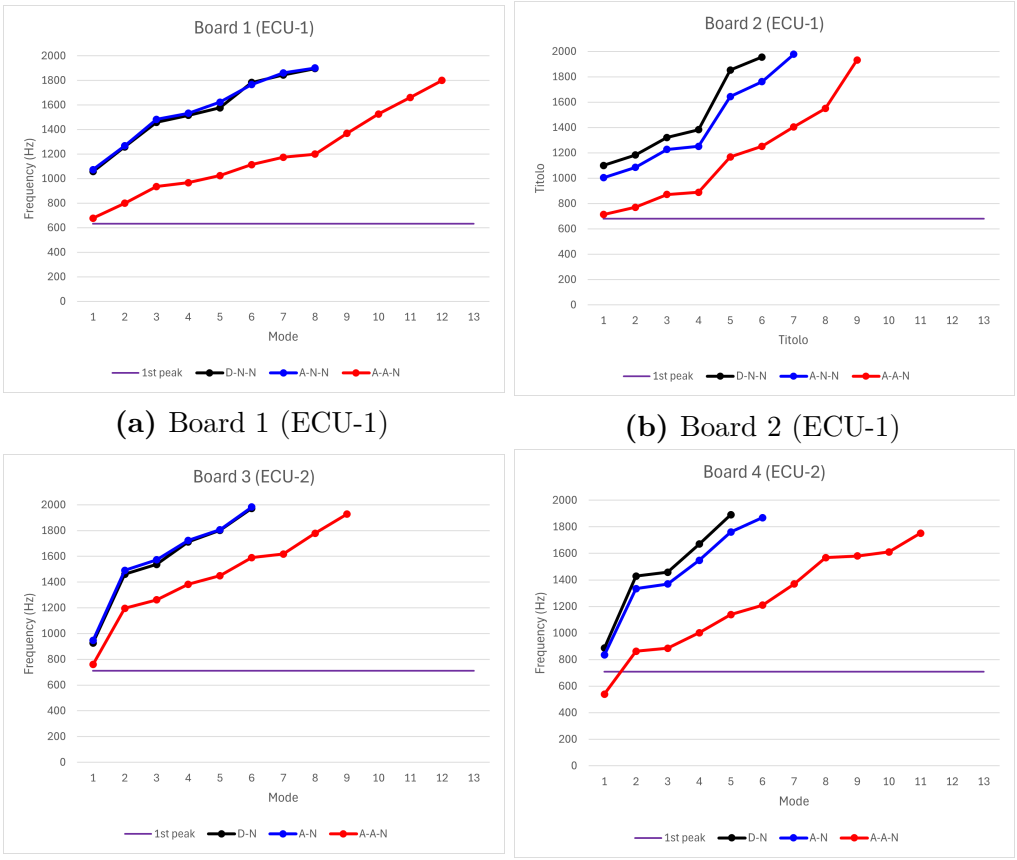

(a) Board 1 (ECU-1)

(b) Board 2 (ECU-1)

(c) Board 3 (ECU-2)

(d) Board 4 (ECU-2)

Figure 3.12: Modes of the different models of the four Boards up to 2000 Hz

and Figure 3.13, it can be observed that the A–A–N model (red line) provides the closest correlation with the experimental results. For the first three boards, the predicted first natural frequency matches the measured value with very limited deviation, while for the fourth board a larger discrepancy is observed.

The comparison between the experimental first natural frequency and the numerical results obtained with the A–A–N model is summarized in Table 3.8. The first three boards show good agreement, with an average deviation below 7%. The fourth board, however, exhibits a significantly lower numerical value, likely due to

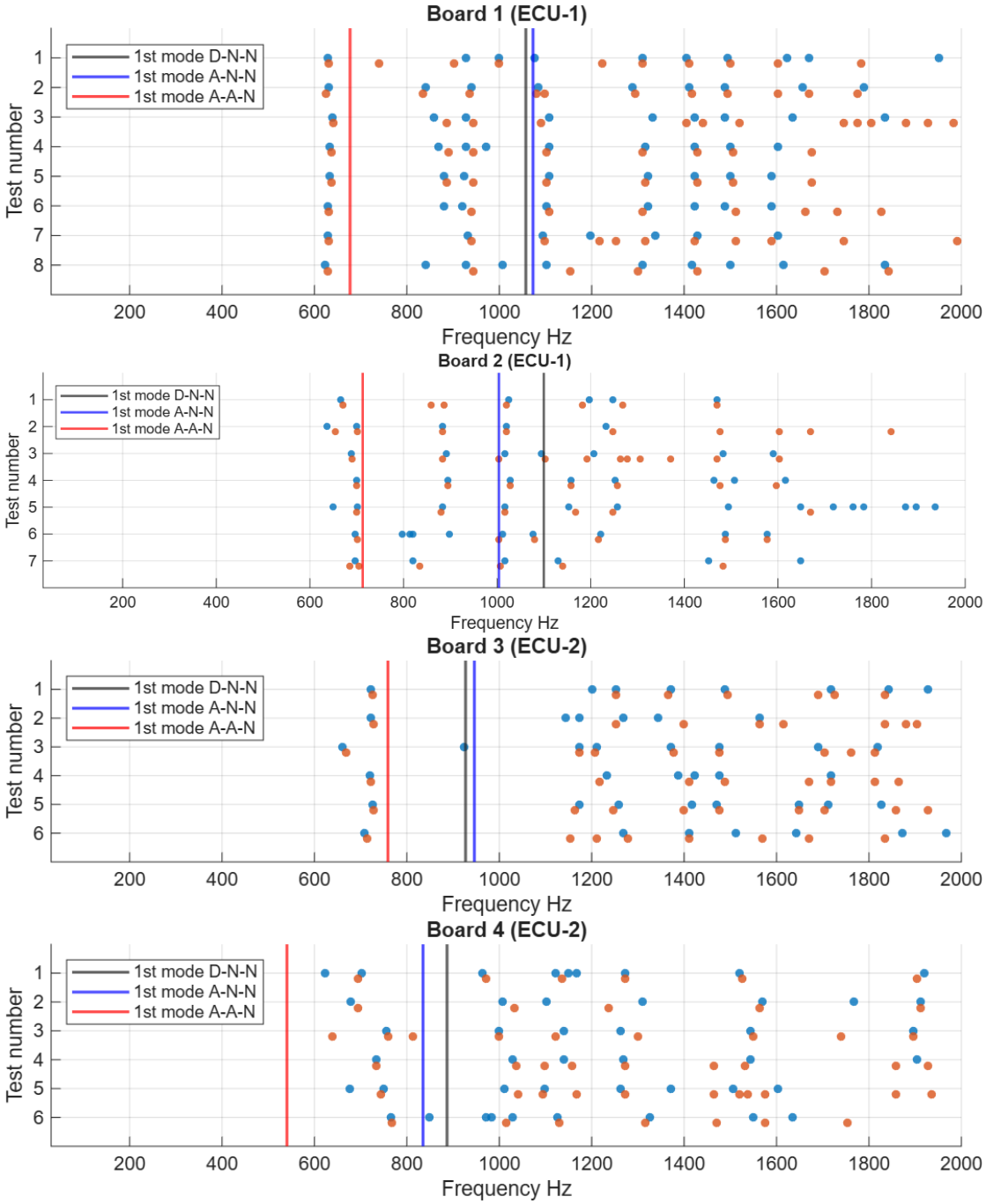

Figure 3.13: Modes of the different models of the four Boards up to 2000 Hz

local differences in mass distribution.

BOARD	1st PEAK	1st MODE A-A-N	error
1	632	676,99	7%
2	681	712,91	5%
3	712	759,47	7%
4	709	540,41	-24%

Table 3.8: Summary of A-A-N versus experimental results

3.4 Conclusions

The numerical investigation demonstrated that simplified finite element models can provide a reliable estimation of the fundamental frequency of printed circuit assemblies, provided that the main structural characteristics are properly represented.

Among the developed models, the A–A–N configuration showed the best correlation with the experimental data, reproducing the first natural frequency with an average error below 7% for three out of four boards. The inclusion of the component masses was proved essential to achieve this level of accuracy, while the models neglecting such contribution (D–N–N and A–N–N) systematically overestimated the stiffness of the assemblies.

In the following chapter the validated model (A-A-N), is employed to investigate the influence of the number and position of the supports on the dynamic response of the assembly, with the objective of identifying an optimal support configuration capable of maximizing the fundamental frequency.

Chapter 4

Support Placement Optimization

In this chapter, the optimization of the support placement for rectangular PCAs is presented. The objective is to identify the most effective number and position of point supports in order to maximize the board first natural frequency.

4.1 State of Art

The problem of determining the optimal number and placement of point supports for PCAs (Printed Circuit Assemblies) involves several complex aspects. First of all, a Printed Circuit Board (PCB) constrained by discrete point supports has no general analytical solution, unlike boards constrained along their edges. Therefore, it is necessary to simulate the PCB dynamic behavior using finite element (FEM) analysis.

However, in most real PCA design cases, there is not enough time available to perform detailed simulations for every configuration. Steinberg [11] presented a set of natural frequencies for various PCB geometries with different support configurations, computed using numerical methods. Figure 4.1 reports the first three natural frequencies for rectangular, uniform PCBs with several types of support layouts, as derived from Steinberg [11].

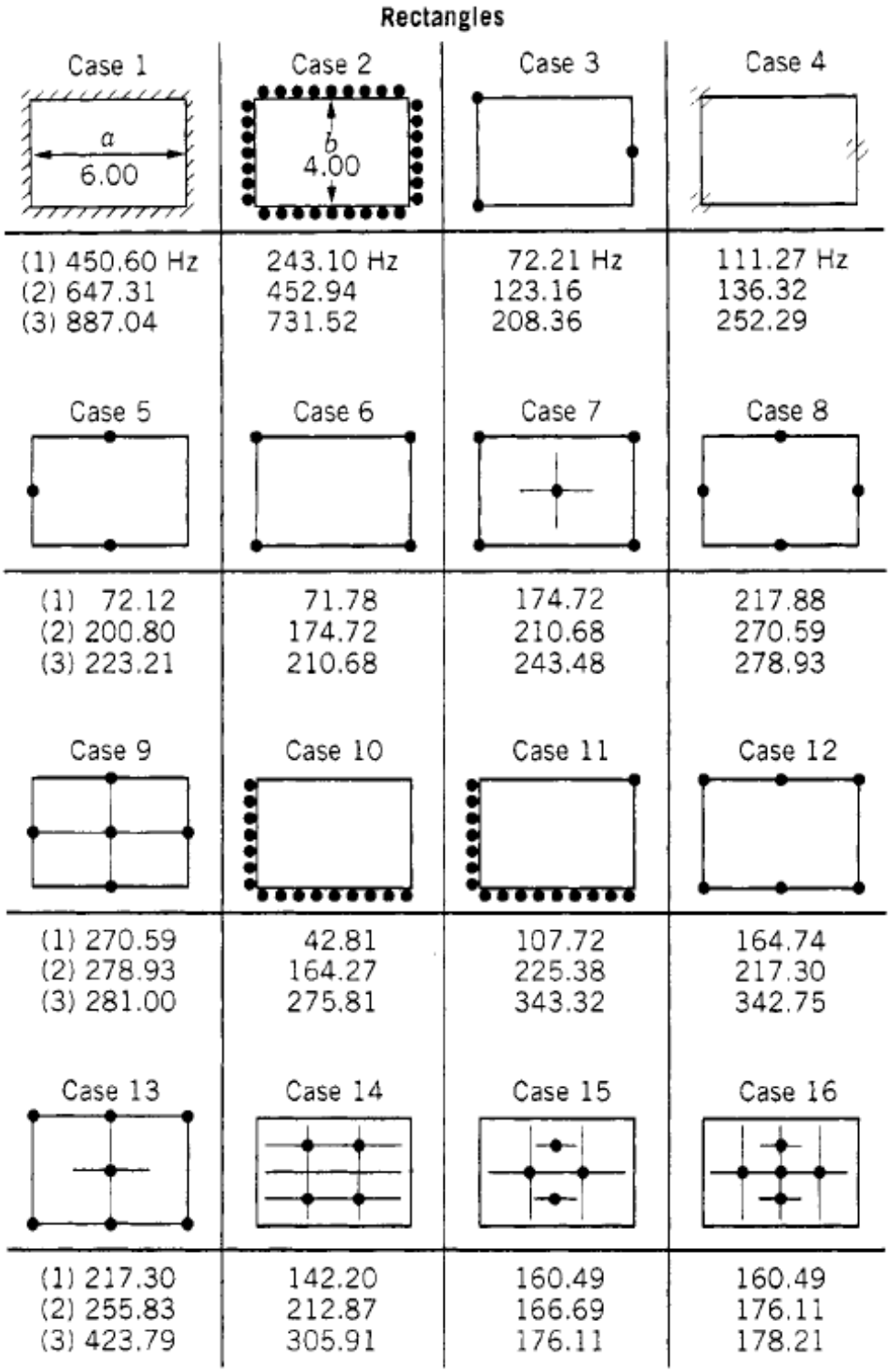

Figure 4.1: Natural frequencies for flat uniform rectangular plates with different types of supports [11]

The results presented by Steinberg are valid only for plates having the same characteristics used in the original FEM models. However since the mode shapes of a board depend solely on its geometry and boundary conditions, the natural frequencies for PCBs with similar shapes and support configurations, but different sizes or materials, can be estimated using the scaling relationship given by Equation 4.1 [11].

$$f_2 = f_1 \left(\frac{a_1 b_1}{a_2 b_2} \right) \sqrt{\frac{E_2 \left(t_2\right)^2 \rho_1 \left[1 - \left(\nu_1\right)^2\right]}{E_1 \left(t_1\right)^2 \rho_2 \left[1 - \left(\nu_2\right)^2\right]}} \tag{4.1}$$

Where:

- f (natural frequency [Hz])
- a (long side)
- b (short side)
- E (Young's modulus)
- t (thickness)
- ρ (density)
- ν (Poisson's ratio)

Blevins [7] expressed plate natural frequencies in terms of a λ (dimensionless natural frequency parameter):

$$f_{ij} = \frac{\lambda_{ij}^2}{2\pi a^2} \sqrt{\frac{Et^3}{12\gamma \left(1 - \nu^2\right)}} \tag{4.2}$$

mass per unit area is computed as $\gamma = \rho \cdot t$ while $i = 1, 2, 3, \ldots$ and $j = 1, 2, 3, \ldots$ describe the number of half waves in the mode shape along the two sides of the plate as shown in Figure 4.2.

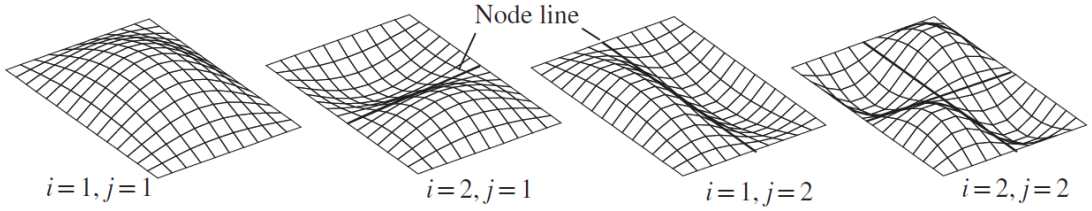

Figure 4.2: First four modes of simply supported rectangular plate [7]

Blevins also presented a series of cases for plates with different boundary and support conditions, providing the corresponding values of λ^2. Two configurations of the ones proposed by Blevins are shown in Figure 4.3.

Natural Frequency, $f_{ij} = \frac{\lambda_{ij}^2}{2\pi a^2}\left[\frac{Eh^3}{12\gamma(1-\nu^2)}\right]^{1/2}$ Hz, i = 1,2,3..; j = 1,2,3...

Boundary Conditions	Natural Frequency Parameter, λ^2
22. Corner Point Supports 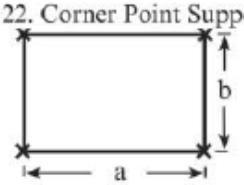	ν=0.3 Ref. [65] a/b | 1 | 1.5 | 2.0 | 2.5 λ_1^2 | 7.12 | 8.92 | 9.29 | 9.39 λ_2^2 | 15.8 | 21.5 | 27.5 | 35.5 Point supports allow rotation but not out-of-plane displacement.
23. Square Plate with Four Point Supports 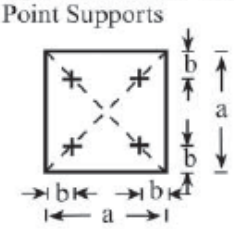	ν=0.3 Ref. [66] b/a | 0 | 0.1 | 0.2 | 0.3 | 0.4 | 0.5 λ_1^2 | 7.14 | 12.89 | 19.69 | 19.31 | 13.35 | 11.34 λ_2^2 | 15.79 | 19.69 | 23.13 | 19.72 | 14.06 | 13.47 λ_3^2 | 19.69 | 23.97 | 32.56 | 24.30 | 16.83 | 19.69 b/a=0.5 gives a single point support at center of plate.

Figure 4.3: Natural frequency of rectangular plates constrained with point supports [7]

In conclusion, to predict the natural frequency of a board constrained by point supports, it is necessary to have a reference solved model sharing the same topology, that is, the same aspect ratio and relative support placement. If the dimensionless natural frequency parameter λ is known for such a configuration, the actual frequency can be computed for boards of any size and material using the corresponding scaling relations.

4.2 Optimization Methodology

4.2.1 Design Constraints and Parameters

To define guidelines for the number and placement of supports for PCAs similar to the ones analyzed in the previous chapter, it is important to understand the constraints governing support placement.

First, the PCB is populated with copper traces and placing all supports in the

middle of the board would greatly complicate the routing process. Therefore, it is standard practice to place supports as close as possible to the edges. However, some supports are sometimes placed in central areas when necessary, though their number is usually limited.

Another constraint arises from the presence of board-to-board perpendicular connectors, which must be positioned along the board edges, generally on the longer side. Consequently, the supports near these edges must be adequately spaced from the edge and leave room for the connectors.

Finally, an important design parameter is the aspect ratio between the board's sides. It is not feasible to cover all possible ratios, but by selecting a representative aspect ratio, it is possible to represent most applications toward which this optimization is targeted.

4.2.2 Baseline model

The baseline PCB geometry used for optimization is shown in Figure 4.4. It represents a rectangular board with dimensions $a = 120$ mm and $b = 110$ mm, corresponding approximately to the average dimensions of the studied PCAs.

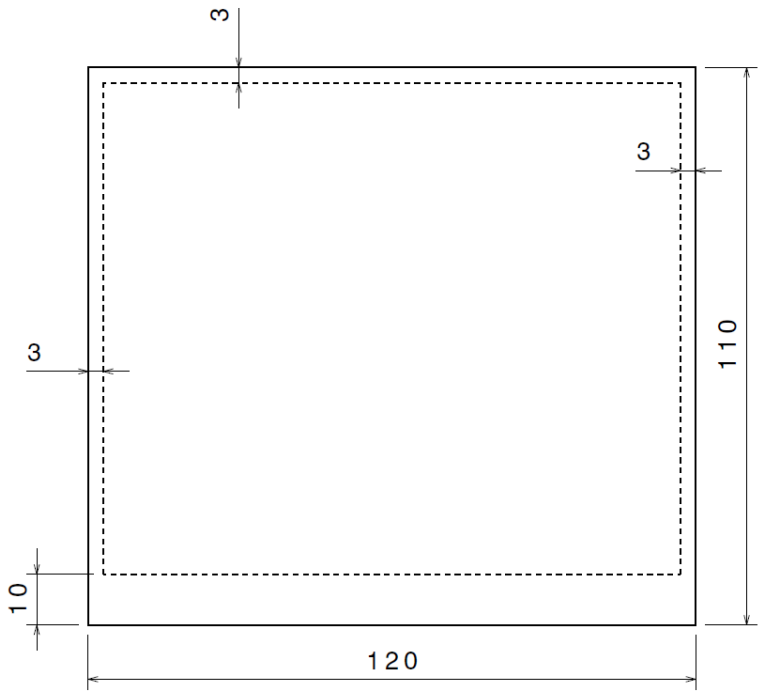

Figure 4.4: Optimization scheme (mm)

The dashed lines in Figure 4.4 indicate the preferred locations of the supports;

along the edges. Supports are positioned 10 mm from one of the longer sides to allow space for potential board-to-board perpendicular connectors, and 3 mm from the remaining edges to accommodate screw holes for M2.5 screws (diameter 2.69 mm).

Once the geometry is defined, other properties such as plate thickness and material parameters (Young's modulus, Poisson's ratio, and density) can be freely chosen, as they do not affect the dimensionless parameter λ.

For the material properties in Equation 4.2, a homogenized A-A-N model is used (Averaged PCB properties, Averaged components mass, Neglected components stiffness). In this model, the Young's modulus and Poisson's ratio ratio are calculated as weighted averages of copper and FR4, while the total mass accounts for both the PCB and mounted components.

The properties are therefore:

$$E = x_{\mathrm{Cu}} \cdot E_{\mathrm{Cu}} + (1 - x_{\mathrm{Cu}}) \cdot E_{\mathrm{FR4}} \tag{4.3}$$

$$\gamma = \frac{m_{\mathrm{tot}}}{A_{\mathrm{PCB}}} \tag{4.4}$$

$$\nu = x_{\mathrm{Cu}} \cdot \nu_{\mathrm{Cu}} + (1 - x_{\mathrm{Cu}}) \cdot \nu_{\mathrm{FR4}} \tag{4.5}$$

And the Equation 4.2 can be rewritten as:

$$f = \frac{\lambda^2}{2\pi a^2} \sqrt{\frac{\left[x_{\mathrm{Cu}} \cdot E_{\mathrm{Cu}} + (1 - x_{\mathrm{Cu}}) \cdot E_{\mathrm{FR4}}\right] \; t^3}{12 \left(\frac{m_{\mathrm{tot}}}{A_{\mathrm{PCB}}}\right) \left(1 - \left[x_{\mathrm{Cu}} \cdot \nu_{\mathrm{Cu}} + (1 - x_{\mathrm{Cu}}) \cdot \nu_{\mathrm{FR4}}\right]^2\right)}} \tag{4.6}$$

To calculate the first natural frequency for a PCB with known topology (and therefore known γ), the required inputs are: the material properties of copper and FR4, the copper volume fraction, the PCB area, the PCB thickness, and the total PCA mass.

The parameter a in Equation 4.6 allows scaling of the formula with PCB geometry: the frequency is related to dimension a through an inverse square relationship. In practice, however, this is not fully realistic because features such as the space required for connectors and screw holes, are absolute and do not scale proportionally with the board dimensions.

For the initial optimization simulation, the properties in Equation 4.6 must be defined. The copper and FR4 material properties are given in Table 3.4. The baseline PCB area is defined by the geometry in Figure 4.4, with $a = 120$ mm and $b = 110$ mm, values chosen as approximate averages of the studied PCAs. Using the same approach, the thickness is set to 1.7 mm, the mass is 97.5 g, and the copper fraction is 8.62%.

4.2.3 FEM optimization

The optimization of support locations is carried out using the ANSYS optimization tool. First, the number of supports to be optimized is determined. The supports are then positioned based on one or more design parameters.

The coordinate system was chosen to simplify the optimization process, with the origin placed at the center of the PCB.

Four lateral supports

The optimization of the configuration with four lateral supports, without any central support, was performed starting from the baseline model described previously. Circular holes with a diameter of 2.69 mm, corresponding to the mounting screw holes, were introduced along the edges of the board.

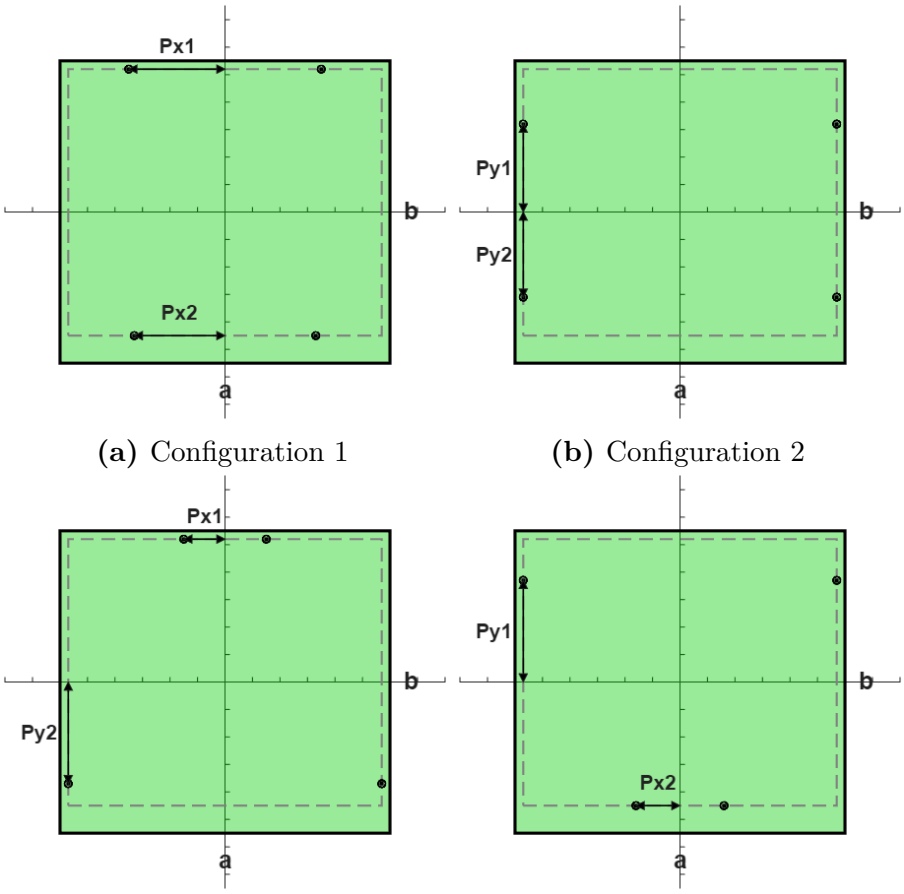

(a) Configuration 1 **(b)** Configuration 2

(c) Configuration 3 **(d)** Configuration 4

Figure 4.5: Four lateral supports optimization configurations

Their positions were defined as functions of the design parameters shown in Figure 4.5. These parameters were then optimized using the ANSYS optimization tool to identify the configuration characterized by the highest first natural frequency.

Table 4.1 presents the optimized configurations together with the corresponding parameter values and the dimensionless natural frequency parameter λ.

Then to the previous configurations a central support was added on the symmetry axis (Figure 4.6) and is position was optimized together with the other four, the output is reported in Table 4.1.

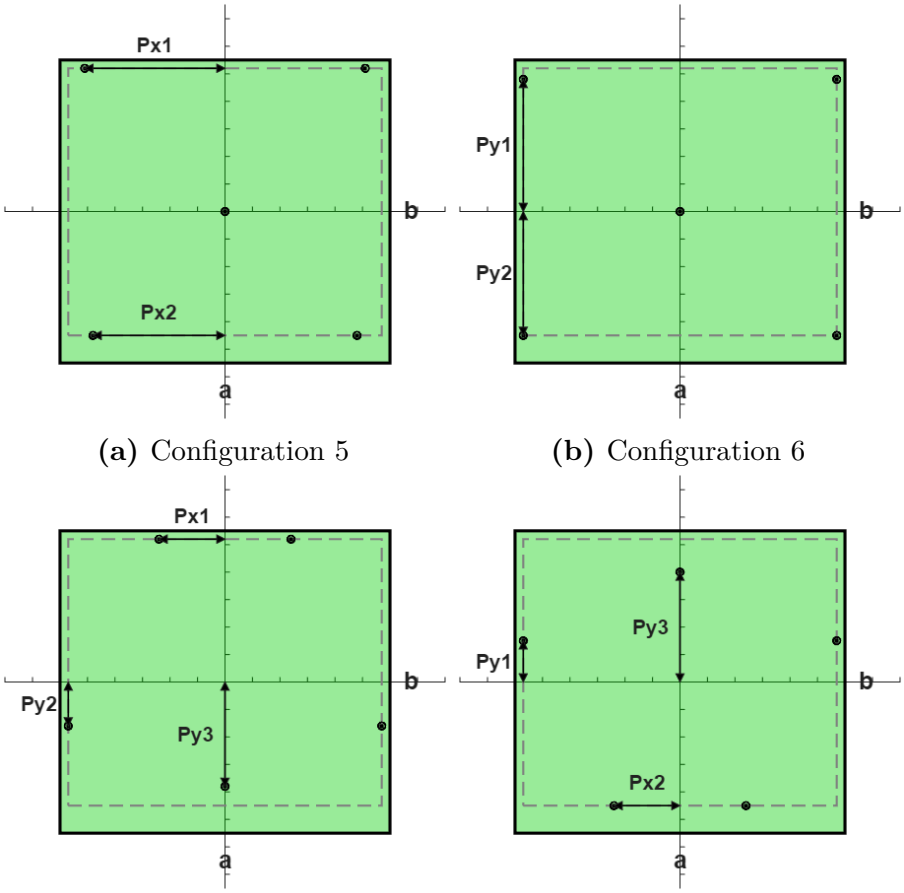

(a) Configuration 5 **(b)** Configuration 6

(c) Configuration 7 **(d)** Configuration 8

Figure 4.6: Four lateral supports plus one central support optimization configurations

				Number of supports		
Configuration	Figure	$\boldsymbol{\lambda^2}$	Parameters	Lateral	Central	Total
1	4.5a	**24.02**	Px1= $0.29\,a$ Px2= $0.28\,a$	4	0	4
2	4.5b	**17.22**	Py1= $0.29\,b$ Py2= $0.28\,b$	4	0	4
3	4.5c	**19.24**	Px1= $0.13\,a$ Py2= $0.34\,b$	4	0	4
4	4.5d	**20.11**	Px2= $0.13\,a$ Py1= $0.35\,b$	4	0	4
5	4.6a	**33.71**	Px1= $0.43\,a$ Px2= $0.40\,a$	4	1	5
6	4.6b	**28.21**	Py1= $0.44\,b$ Py2= $0.41\,b$	4	1	5
7	4.6c	**31.54**	Px1= $0.20\,a$ Py2= $0.15\,b$ Py3= $0.35\,b$	4	1	5
8	4.6d	**31.61**	Px2= $0.20\,a$ Py1= $0.13\,b$ Py3= $0.36\,b$	4	1	5

Table 4.1: Parametric summary of the optimized configurations for a board constrained by four lateral supports $a = 120,\ b = 110$

Among the configurations with four lateral supports only (Configurations 1–4), the obtained λ^2 values range approximately between 17 and 24. In these cases, the absence of a central constraint allows larger global deformations of the board, which results in lower natural frequencies. When a central support is added (Configurations 5–8), λ^2 increases, reaching values between 28 and 34. The highest value of λ^2 is obtained for Configuration 5.

Six lateral supports

A similar procedure was adopted to optimize configurations characterized by six lateral supports. The first four configuration (Figure 4.7) are generated by adding two supports first on the vertical axis, then on the horizontal axis of the first two configuration in Figure 4.5.

A central support was then added to each of the four selected configurations, as shown in Figure 4.8, and its position was fixed at the center of the board.

The results from the optimization of the eight configurations are reported in Table 4.2.

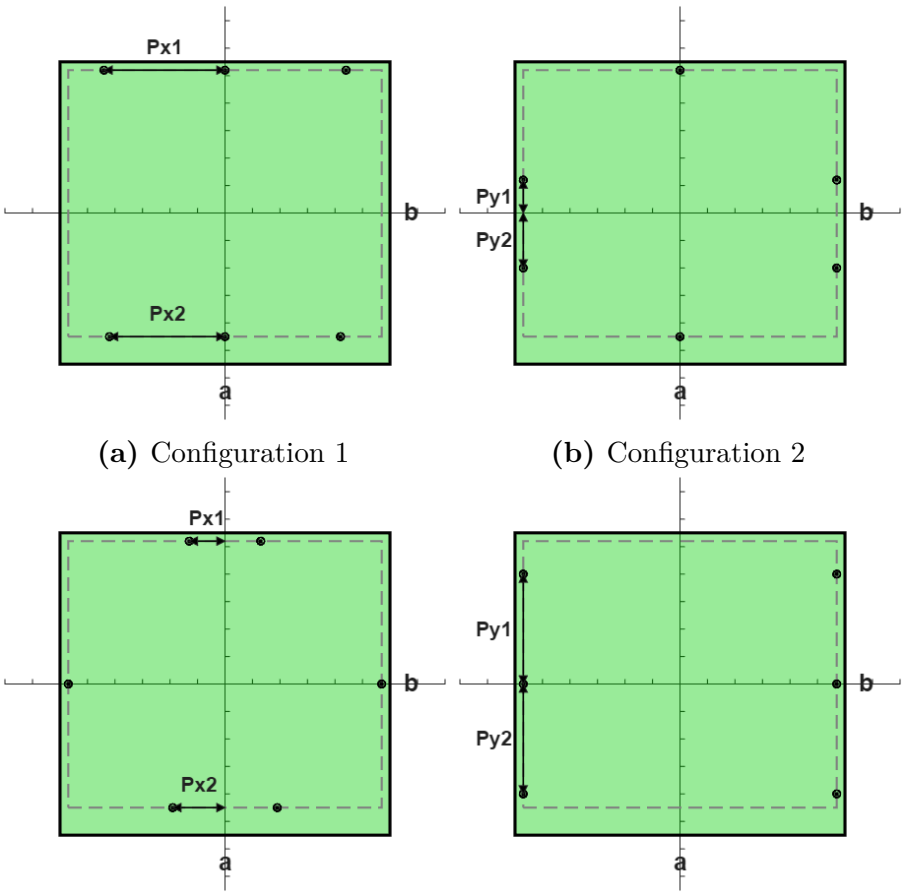

(a) Configuration 1 **(b)** Configuration 2

(c) Configuration 3 **(d)** Configuration 4

Figure 4.7: Six lateral supports optimization configurations

It can be observed that the first four configurations, featuring six supports along the edges only, show λ^2 values that are generally higher but still comparable to those obtained with the four edge support configurations. When a central support is added (Configurations 5–8), the λ^2 values further increase; however, the real advantage is achieved only when the additional supports are strategically positioned. In particular, Configurations 6 and 7 exhibit the highest performance, with λ^2. and therefore the fundamental frequency, increasing by approximately 47% compared to the best among the remaining configurations.

These results demonstrate that the benefit of adding supports strongly depends on their placement rather than their number. For example, Configuration 5 has a lower λ^2 value than Configuration 3 despite more supports. Similarly, in the four-support case (Figure 4.6a), Configuration 5, with $\lambda^2 = 33$, achieves a higher fundamental frequency than Configuration 4, which includes one additional support.

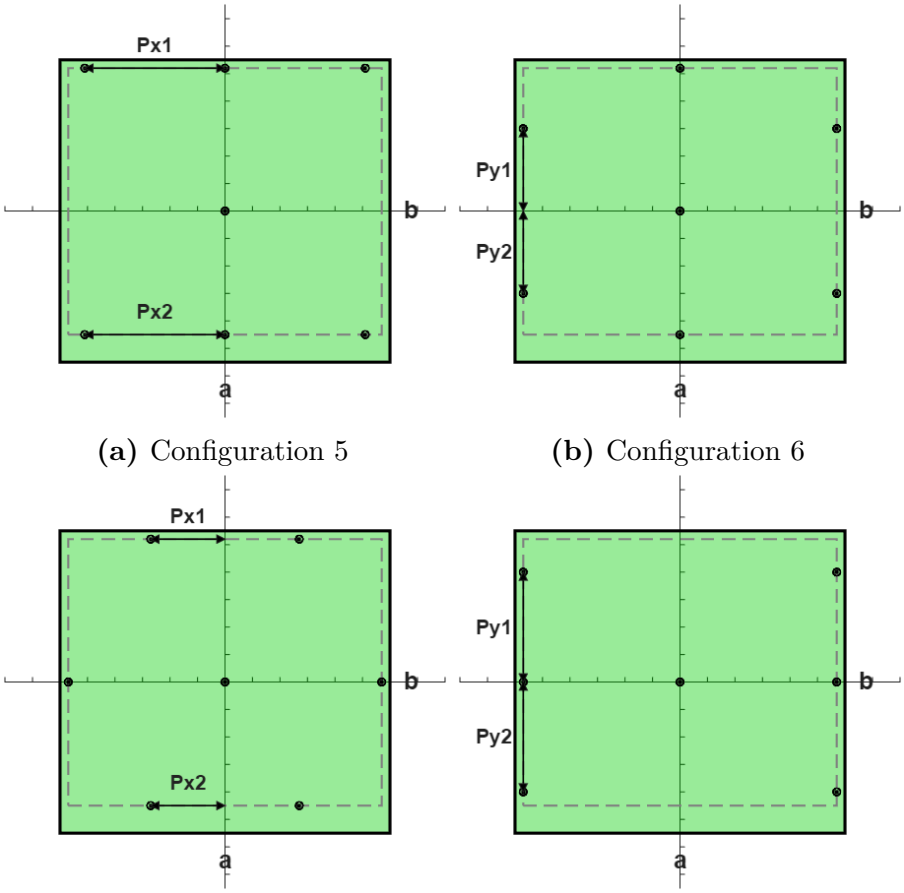

(a) Configuration 5 **(b)** Configuration 6

(c) Configuration 7 **(d)** Configuration 8

Figure 4.8: Six lateral supports plus one central support optimization configurations

4.3 Application example of the proposed method

To demonstrate the practical use of the proposed optimization approach, an example application is presented in this section. The goal is to design a PCA whose first natural frequency exceeds 600 Hz, by selecting an appropriate support configuration from the optimized topologies previously obtained.

The design starts from the basic information typically available during the early design phase: the geometric dimensions of the PCB, the copper percentage, and the estimated total mass of the assembled PCA. The material properties of copper and FR4 are known and reported in Table 4.3.

				Number of supports		
Configuration	Figure	$\boldsymbol{\lambda^2}$	Parameters	Lateral	Central	Total
1	4.7a	**25.54**	Px1= $0.37\,a$ Px2= $0.35\,a$	6	0	6
2	4.7b	**34**	Py1= $0.11\,b$ Py2= $0.18\,b$	6	0	6
3	4.7b	**34.15**	Px1= $0.11\,a$ Px2= $0.16\,a$	6	0	6
4	4.7b	**19.17**	Py1= $0.36\,a$ Py2= $0.36\,a$	6	0	6
5	4.7b	**34**	Px1= $0.43\,a$ Px2= $0.43\,a$	6	1	6
6	4.7b	**56.57**	Py1= $0.27\,b$ Py2= $0.27\,b$	6	1	6
7	4.7b	**50.35**	Px1= $0.23\,a$ Px2= $0.23\,a$	6	1	6
8	4.7b	**28.29**	Py1= $0.36\,b$ Py2= $0.36\,b$	6	1	6

Table 4.2: Parametric summary of the optimized configurations for a board constrained by six lateral supports $a = 120,\ b = 110$

Parameter	**Symbol**	**Value**
PCB length	a	120 mm
PCB width	b	110 mm
PCB thickness	t	1.8 mm
Copper fraction	x_{Cu}	10%
Total mass of PCA	m_{tot}	0.090 kg
Density of copper	ρ_{Cu}	8300 kg/m^3
Young's modulus of copper	E_{Cu}	110 GPa
Poisson's ratio of copper	ν_{Cu}	0.34
Density of FR4	ρ_{FR4}	1850 kg/m^3
Young's modulus of FR4	E_{FR4}	19.45 GPa
Poisson's ratio of FR4	ν_{FR4}	0.17

Table 4.3: Input data for the optimization example

From these data, assuming the target first natural frequency is $f_1 \geq 600$ Hz, Equation 4.6 can be rearranged in Equation 4.7 employed to compute the corresponding λ^2:

$$\lambda^2 = 2\pi a^2 f_1 \sqrt{\frac{12\left(\frac{m_{\text{tot}}}{A_{\text{PCB}}}\right)\left(1-\left[x_{\text{Cu}}\cdot\nu_{\text{Cu}}+(1-x_{\text{Cu}})\cdot\nu_{\text{FR4}}\right]^2\right)}{\left[x_{\text{Cu}}\cdot E_{\text{Cu}}+(1-x_{\text{Cu}})\cdot E_{\text{FR4}}\right]\ t^3}} = 37.41 \qquad (4.7)$$

The resulting value serves as a reference for selecting an optimized support configuration from the available topologies.

Among the configurations analyzed in the optimization study, those with a λ^2 value equal to or greater than 37.41 are considered suitable candidates. From Table 4.1, it can be observed that none of the configurations featuring only four lateral supports satisfy this requirement. In contrast, Table 4.2 shows that Configurations 6 and 7 both achieve sufficiently high λ^2 values.

The final choice, however, depends not only on dynamic performance but also on practical considerations such as component layout and available mounting space. Since both Configuration 6 and 7 include six lateral supports and one central support, Configuration 6 is the most advisable option, as it features the highest λ^2 value,approximately 51% higher than the minimum required threshold.

To validate the methodology, a FEM model was created using the material and geometric properties reported in Table 4.3, adopting the layout of Configuration 6 from Table 4.2. A modal analysis was then performed to determine the first natural frequency, which was compared to the target value and to the analytical estimate.

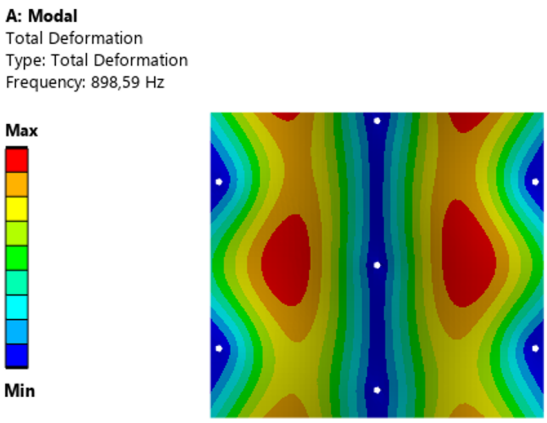

Figure 4.9: First mode shape of the application example

As shown in Figure 4.9, the first mode occurs at a natural frequency of 899 Hz, approximately 50% higher than the target frequency of 600 Hz. This confirms the proportional relationship between λ^2 and the resulting natural frequency.

This example illustrates how the proposed optimization method can be applied in the design process, providing a structured way to predict the board's dynamic response.

Chapter 5

Conclusion

This thesis addressed the problem of optimizing the placement of point supports for rectangular Printed Circuit Assemblies, with the primary goal of maximizing the first natural frequency.

Experimental results showed that, despite differences among the boards, the first natural frequency consistently falls within the range of approximately 600-800 Hz, giving a solid base for future design considerations.

Through the development of FEM models, a homogeneous model was identified to adequately represent the dynamic behavior of this type of PCAs. The model distributes the mechanical properties of the PCBs uniformly across the board and features an equivalent density representing the total mass of the PCAs, including mounted components. This approach enables accurate simulation of the first natural frequency without modeling every geometric detail of the real board.

Another important result is the relationship between the physical properties of the board and its natural frequency. It was shown that, starting from uniform boards, the natural frequency of a given mode shape can be correlated with parameters such as density, thickness, copper fraction, and total mass of the PCA. This relationship includes a dimensionless parameter λ, whose squared value is proportional to the corresponding frequency, which depends on the board's aspect ratio and the placement of supports, providing a theoretical reference for comparing different configurations.

The optimization work consisted of developing, modeling, and optimizing various support topologies, evaluating their impact on the natural frequency, and reporting the corresponding λ values.

The parameter λ can therefore be used as a reference indicator during the design phase: once the desired first natural frequency and the main physical properties of a PCA are known, the required λ^2 value for that PCA can be computed. Designers can then select the most appropriate support configuration among the optimized topologies presented in this work, choosing the one whose λ^2 value meets or exceeds

the required threshold while best fitting the mechanical and geometric constraints of the specific application.

While the presented methodology provides a useful design reference, there is still room for improvement and further development of this work. From an experimental point of view, using non contact measurement techniques such as laser vibrometers would allow more accurate results by avoiding the mass effect of traditional accelerometers on the dynamic response of the PCA. Testing a larger number of boards would also make the results more reliable, improving the statistical accuracy of the measured frequencies.

Then, the FEM models could be refined by directly measuring the mechanical properties of the PCB materials instead of relying on estimated values from datasheet that are often incomplete. This would lead to a more realistic representation of the actual behavior of the boards.

Another important development would be to extend the optimization study to include a wider range of support configurations, allowing the determination of new and higher λ^2 values for more complex or demaning layouts.

Finally, during the design phase of a PCA, not all the parameters required for applying the proposed optimization method are usually known in advance. For example, the total mass of the assembled board is often available only after manufacturing. A possible development would be to simulate the design process itself, using statistical estimation of unknown quantities such as total mass, based on data collected from a larger set of PCAs. This would make the optimization approach more practical and directly applicable to real design situations.

Overall, the findings presented in this thesis contribute to a more structured and objective understanding of the dynamic behavior of printed circuit assemblies, providing a basis for their future design and analysis.

Bibliography

[1] Leonard Marks and James Caterina. *Printed Circuit Assembly Design*. McGraw-Hill, 2000 (cit. on p. 1).

[2] R.S. Khandpur. *Printed Circuit Boards: Design, Fabrication, Assembly and Testing*. McGraw-Hill, 2006. ISBN: 9780070588141. URL: https://books.google.it/books?id=VY8iBAAAQBAJ (cit. on pp. 2, 3, 5).

[3] *Board-to-Board Connector*. https://www.greenconn.com/en/board-to-board-connectors.htm. Accessed: 2025-07-31 (cit. on p. 6).

[4] Jerrod P Peterson. «Finite element techniques for modeling the effect on circuit board dynamic response of mechanical coupling at electrical board-to-board connectors.» In: Sandia National Lab. (SNL-CA), Livermore, CA (United States). Dec. 2010. URL: https://www.osti.gov/biblio/1673897 (cit. on p. 7).

[5] *Understanding the Role of Thermal Pads in PCB Cooling*. https://jlcpcb.com/blog/understanding-the-role-of-thermal-pads-in-pcb-cooling. Accessed: 2025-07-31 (cit. on p. 8).

[6] S.S. Rao. *Mechanical Vibrations*. Pearson Education, Incorporated, 2017. ISBN: 9780134361307. URL: https://books.google.it/books?id=t6gHswEACAAJ (cit. on pp. 9, 10).

[7] Robert Blevins. *Formulas for Dynamics, Acoustics and Vibration*. Nov. 2015, pp. 1–448. ISBN: 9781119038115. DOI: 10.1002/9781119038122 (cit. on pp. 11, 51, 52).

[8] J. M. Pitarresi and A. A. Primavera. «Comparison of Modeling Techniques for the Vibration Analysis of Printed Circuit Cards». In: *Journal of Electronic Packaging* 114.4 (Dec. 1992), pp. 378–383 (cit. on p. 31).

[9] Robin Alastair Amy, G.S. Aglietti, and Guy Richardson. «Sensitivity analysis of simplified Printed Circuit Board finite element models». In: *Microelectronics Reliability* 49.7 (2009), pp. 791–799 (cit. on p. 33).

[10] Venkat, P. Rao, Arun Singh, Srikrishna Parthasarathi, and Ranganath. «Vibration Analysis of Printed Circuit Board Plate with Varying Boundary Conditions». In: *Indian Journal of Science and Technology* 9 (Sept. 2016) (cit. on p. 35).

[11] Dave S. Steinberg. *Vibration Analysis for electronic equipment*. John Wiley & Sons, 2000 (cit. on pp. 35, 49–51).

[12] Kun-Nan Chen. «Optimal Support Locations for a Printed Circuit Board Loaded With Heavy Components». In: *Journal of Electronic Packaging - J ELECTRON PACKAGING* 128 (Dec. 2006). DOI: 10.1115/1.2353281 (cit. on p. 35).

[13] Robin Alastair Amy, Guglielmo S. Aglietti, and Guy Richardson. «Accuracy of simplified printed circuit board finite element models». In: *Microelectronics Reliability* 50.1 (2010), pp. 86–97. ISSN: 0026-2714. DOI: https://doi.org/10.1016/j.microrel.2009.09.001. URL: https://www.sciencedirect.com/science/article/pii/S0026271409003515 (cit. on p. 35).

[14] Faical Arabi, Alexandrine Gracia, Jean-Yves Deletage, and Helene Fremont. «Vibration test and simulation of printed circuit board». In: Apr. 2018, pp. 1–7. DOI: 10.1109/EuroSimE.2018.8369909 (cit. on pp. 35, 36).